Contribution of the clathrin adaptor AP-1 subunit μ1 to acidic cluster protein sorting

Paloma Navarro Negredo, James R. Edgar, Antoni G. Wrobel, Nathan R. Zaccai, Robin Antrobus, David J. Owen, and Margaret S. Robinson

Cambridge Institute for Medical Research, University of Cambridge, Cambridge, England, UK

Acidic clusters act as sorting signals for packaging cargo into clathrin-coated vesicles (CCVs), and also facilitate down-regulation of MHC-I by HIV-1 Nef. To find acidic cluster sorting machinery, we performed a gene-trap screen and identified the medium subunit (μ1) of the clathrin adaptor AP-1 as a top hit. In μ1 knockout cells, intracellular CCVs still form, but acidic cluster proteins are depleted, although several other CCV components were either unaffected or increased, indicating that cells can compensate for long-term loss of AP-1. In vitro experiments showed that the basic patch on μ1 that interacts with the Nef acidic cluster also contributes to the binding of endogenous acidic cluster proteins. Surprisingly, μ1 mutant proteins lacking the basic patch and/or the tyrosine-based motif binding pocket could rescue the μ1 knockout phenotype completely. In contrast, these mutants failed to rescue Nef-induced down-regulation of MHC class I, suggesting a possible mechanism for attacking the virus while sparing the host cell.

Introduction

Vesicle trafficking is essential for the normal exchange of proteins and lipids between intracellular membrane compartments and is also frequently exploited by pathogens. Clathrin-coated vesicles (CCVs) are among the most abundant and versatile vesicles in the cell, mediating both endocytosis and transport between the TGN and endosomes (Robinson, 2015). Packaging of membrane proteins into CCVs relies on sorting signals in their cytosolic tails, which are usually short linear motifs that bind transiently to proteins called adaptors. The adaptors also interact with clathrin and with one another and thus provide a link between the cargo and the clathrin scaffold.

Several motifs have been shown to be both necessary and sufficient for cargo selection into CCVs, including YXXΦ (where Φ is a bulky hydrophobic residue), [D/E]XXXL[L/I], FXNPXY, DXXLL, and the acidic cluster motif. The YXXΦ and [D/E]XXXL[L/I] motifs are both recognized by the adaptor complexes adaptor protein 1 (AP1) and AP-2, which sort cargo at intracellular membranes and at the plasma membrane, respectively. Both complexes are heterotetramers composed of two large subunits (γ/α and β1/β2), a medium subunit (μ1/μ2), and a small subunit (σ1/σ2). YXXΦ motifs bind to the μ subunits, while [D/E]XXXL[L/I] motifs bind to the σ and γ/α subunits. FXNPXY motifs interact with the phosphotyrosine-binding domains of some of the "alternative adaptors" that act at the plasma membrane, such as Dab2 and ARH, and DXXLL motifs

interact with the GGA family of alternative adaptors, which act at intracellular membranes (Bonifacino and Traub, 2003).

Less is known about how acidic cluster sorting signals are recognized. The first acidic cluster motif to be described was the SDSEEDE sequence in the cytosolic tail of furin, which not only confers TGN localization but also mediates endocytosis at the plasma membrane (Voorhees et al., 1995). Since then, other proteins have been shown to contain acidic cluster sorting signals, including carboxypeptidase D (CPD; Eng et al., 1999) and the cation-independent mannose-6-phosphate receptor (CIMPR) for lysosomal hydrolases (Chen et al., 1997). In addition, the HIV-1 accessory protein Nef has an acidic cluster, which contributes to the down-regulation of MHC class I (MHC-I) from the plasma membrane of infected cells, enabling the virus to evade the immune system of the host (Greenberg et al., 1998). In 1998, PACS-1 (phospho-acidic cluster sorting protein 1) was identified in a yeast two-hybrid screen as a binding partner for the furin cytosolic tail (Wan et al., 1998) and was subsequently reported to facilitate MHC-I down-regulation by Nef (Crump et al., 2001). The authors of these studies proposed that PACS-1 links acidic cluster-containing proteins to AP-1 and thus causes them to become packaged into CCVs. However, other groups have found that PACS-1 does not behave like a CCV-associated protein (Hirst et al., 2012; Borner et al., 2014), that binding of PACS-1 to the Nef acidic cluster is extremely weak (Baugh et al., 2008), and depletion of PACS-1 by siRNA has no effect on either Nef-induced down-regulation of MHC-I

(Lubben et al., 2007) or trafficking of acidic cluster-containing cargo proteins (Harasaki et al., 2005). Thus, although PACS-1 might play a contributory role, it does not appear to be the acidic cluster adaptor.

Studies by Collins and coworkers (Roeth et al., 2004; Wonderlich et al., 2008, 2011), and also from our own laboratory (Lubben et al., 2007), have shown that knocking down AP-1 inhibits MHC-I down-regulation. There are also several studies showing that loss of AP-1 affects the trafficking of acidic cluster-containing cargo proteins (Fölsch et al., 2001; Meyer et al., 2001; Harasaki et al., 2005). Thus, another possibility is that AP-1 itself may be the acidic cluster adaptor. This possibility is supported by a crystal structure of a complex containing the μ subunit of AP-1 (μ1), Nef, and the cytosolic tail of MHC-I, which shows the Nef acidic cluster forming electrostatic interactions with a patch of positively charged residues in the C-terminal μ homology domain (MHD) of μ1 (Jia et al., 2012; Shen et al., 2015). However, the significance of these interactions has not been tested in vivo, so it is still unclear whether AP-1 sorts acidic cluster-containing proteins directly or via another protein or proteins and, if so, what those proteins might be.

We decided to use forward genetics as an unbiased way of potentially identifying both known and unknown proteins. Forward genetic screens have been used for decades on genetically tractable organisms such as yeast, leading to the identification of many important trafficking proteins, most of which are conserved in mammals. Until recently, however, these types of screens were not feasible in human cells, because of their diploid nature. Then in 2009, Carette et al. (2009) showed that forward genetic screens can be performed on a near-haploid human myeloid leukemia line, KBM7, by mutagenesis with a gene-trap virus. Using cell survival as a readout, the authors were able to identify several host factors that are hijacked by pathogens (Carette et al., 2009, 2011; Guimaraes et al., 2011). Subsequent work by Duncan et al. (2012) showed that KBM7 cell mutants can also be selected using flow cytometry, to enrich for cells with increased or decreased surface expression of a protein of interest. Changes in surface expression have historically been used as a readout in screens to identify genes involved in membrane traffic; for instance, many of the yeast vacuolar protein sorting genes were identified by isolating mutants that mislocalized vacuolar proteins to the cell surface (Bankaitis et al., 1986; Robinson et al., 1988). Therefore, we adopted this approach to look for machinery involved in the sorting of acidic cluster-containing proteins.

Results

Forward genetic screens in haploid human cells to identify genes involved in protein trafficking

To generate suitable cell lines for our screens, we stably transduced KBM7 cells with two different constructs, one with an acidic cluster and the other with a YXXΦ motif. Both constructs consist of the extracellular/luminal and transmembrane domains of the T cell protein CD8, which acts as a reporter, fused to distinct cytosolic tails (Fig. 1 a). The CD8-YAAL construct carries a YXXΦ sorting signal surrounded by alanines and was previously used in a genome-wide siRNA library screen (Kozik et al., 2013), so it served as a positive control. The CD8-Furin* construct carries the cytosolic tail of furin, which normally

contains both a YXXΦ motif (YKGL) and an acidic cluster motif. Because we were specifically interested in sorting machinery for the acidic cluster, we mutated the tyrosine residue in the YXXΦ motif to an alanine to render the signal inactive (Lubben et al., 2007).

A schematic diagram of the screening strategy is shown in Fig. 1 b. The two stable cell lines were mutagenized using a gene-trap retrovirus that encodes GFP. When the viral genome inserts into an intron in the right orientation, the presence of a strong splice acceptor site causes the cell to express a GFP-fusion transcript terminated by a stop codon and polyadenylation signal. The loss of transcription of downstream exons creates a null allele, and GFP expression can be used to identify the gene-trapped cells. Two consecutive sorts were performed to isolate GFP-positive cells with either unusually high or unusually low expression of CD8 on the plasma membrane (Fig. 1, b and c). Genomic DNA was then isolated from the cells, sites of retroviral insertion were amplified, and genes containing insertions were identified by deep sequencing. Hits were defined as genes containing more than one disruptive insertion, which were enriched in the sorted population compared with nonselected cells.

For the CD8-YAAL screen, there were no hits identified in the population with decreased surface expression but several in the population with increased surface expression. These included two known components of the clathrin machinery, CALM/PICALM (13 independent insertion sites) and dynamin 2 (DNM2; 6 independent insertion sites), as well as two other proteins involved in trafficking, SORL1 (6 sites) and SEC14L1 (5 sites), thus validating that the gene-trap method can be used to identify trafficking machinery. The CD8-Furin* screen produced only two hits with high surface expression. One was *AP1M1*, the gene encoding AP-1 μ1 (3 sites), and the other was *WDR11* (3 sites), encoding a protein of unknown function (Fig. 1 d). There were also two hits with low surface expression, encoding Rab10 (5 sites), a protein involved in endosomal recycling to the plasma membrane (Shi et al., 2012), and KLHL21 (3 sites), part of an E3 ubiquitin ligase complex (Maerki et al., 2009; Fig. 1 d). Thus, our forward genetic screens yielded both known components of the sorting machinery and potential new players.

Generation of μ1 knockout cells

We decided to focus on μ1 because of previous work suggesting that it might be the acidic cluster adaptor. Attempts to clone μ1-disrupted KBM7 cells were unsuccessful, so we generated μ1 knockout (KO) lines in HeLa cells using CRISPR/Cas9. gRNAs were designed to target exons 2, 3, and 4 of *AP1M1* (Fig. 2 a). After transfection and antibiotic selection, cells were analyzed by immunofluorescence, using an antibody against the AP-1 γ subunit (Fig. 2 b) because there are no suitable antibodies available against μ1. Loss of any one subunit of an AP complex has been shown to render the whole complex inactive (Meyer et al., 2000; Peden et al., 2002), so potential KO cells could be identified in mixed populations by their diffuse cytosolic AP-1 γ labeling (Fig. 2 c, arrows). Such cells were abundant in populations treated with gRNAs targeting exon 2 or 4 but not exon 3. Single-cell clones were isolated from the mixed populations and analyzed by Western blotting, using an antibody raised against the μ subunit of AP-2, which cross-reacts with the μ subunit of AP-1 (Fig. 2 d). In cells lacking μ1, expression of other coat components, including clathrin and GGA2, was found to be normal (Fig. 2 d). Genomic DNA was isolated from
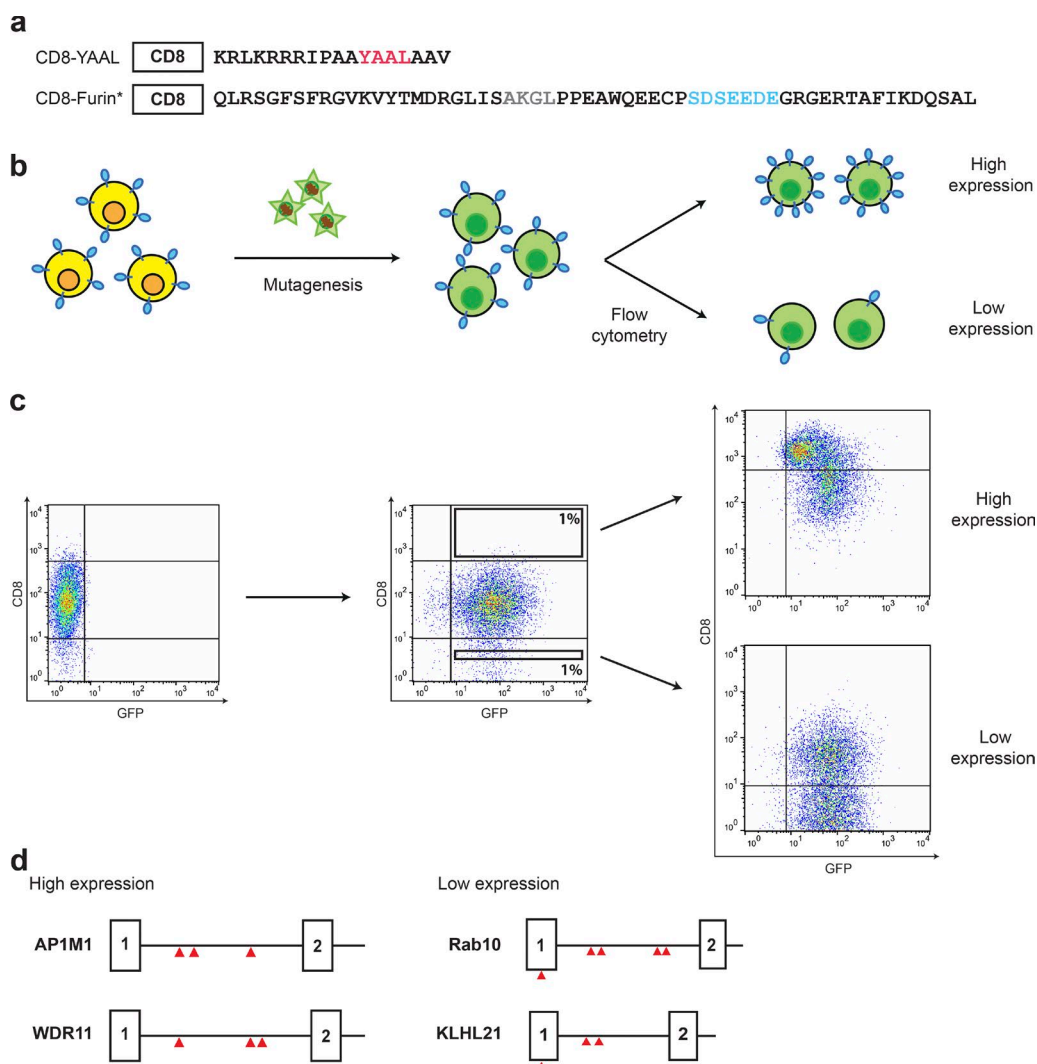
Figure 1. **Haploid forward genetic screens to identify genes involved in protein trafficking.** (a) Cytosolic tail sequences of CD8 chimeras used in the screens. Sorting signals are indicated in color: YXXΦ, pink; acidic cluster, blue; mutated YXXΦ, gray. (b) Schematic diagram of the screening strategy. KBM7 cells stably expressing the CD8 chimeras were mutagenized with a gene-trap retrovirus encoding GFP. GFP-positive cells were sorted for unusually high or low surface levels of CD8 by two consecutive rounds of flow cytometry. (c) FACS plots corresponding to the three stages of the screen shown in b. (d) Hits from the CD8-Furin* screen. The screen identified both known components of the sorting machinery (AP1M1, Rab10) and potential new players (WDR11, KLHL21). Exons are shown as numbered boxes and introns as lines, with red triangles showing independent retroviral integration sites.

two selected clones, one for each gRNA, and sequenced across the region targeted by the gRNAs. In both cases, probable loss-of-function mutations were identified, with no WT sequence remaining (see Materials and methods).

To confirm that loss of μ1 causes an increase in surface expression of acidic cluster–containing proteins, we transiently transfected WT and μ1 KO HeLa cells with the CD8-Furin* plasmid, together with a GFP-encoding plasmid to control for transfection efficiency. Surface labeling for CD8 was analyzed by flow cytometry, gating for GFP-positive cells. There was an approximately twofold increase in surface CD8-Furin* in the μ1 KO cells (Fig. 2 e), validating the KBM7 cell phenotype.

CCVs in μ1 KO cells

Are the μ1 KO cells capable of forming intracellular CCVs? Knocking out *AP1M1* in mice is embryonic lethal, but embryonic fibroblasts have been cultured from the KO mice, and the cells were reported to have no TGN-associated clathrin (Meyer

et al., 2000). However, when we performed electron microscopy on our μ1 KO HeLa cells, we were able to identify clathrin-coated profiles in the TGN region, although they were more difficult to spot than in WT cells because they tended to be smaller (mean diameter 65 vs. 86 nm; Fig. 3, a and b). These are presumably nucleated by some of the alternative adaptors that normally act together with AP-1, such as the GGAs and epsinR. Interestingly, siRNA-mediated depletion of AP-2 from HeLa cells also causes a decrease in the size of clathrin-coated profiles, in this case at the plasma membrane (Motley et al., 2003). In both cases, the reduction in size is probably related to the relatively large "footprints" of the AP complexes on the membrane and the smaller footprints of the alternative adaptors, most of which are monomeric (Hirst et al., 2015; Miller et al., 2015).

We also investigated clathrin localization in living cells, by carrying out spinning disk confocal microscopy on control and μ1 KO cells expressing clathrin light chain conjugated to mCherry. Intracellular clathrin-coated structures can be distin-
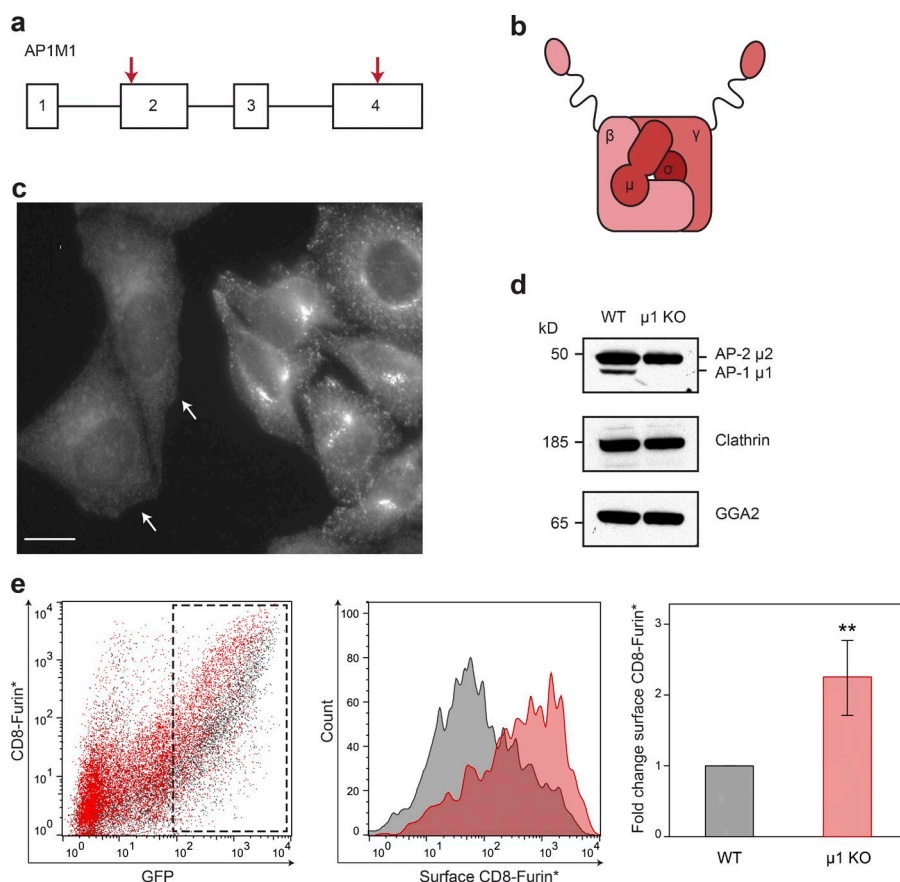
Figure 2. **Generation of μ1 KO cells.** (a) Representation of the *AP1M1* gene showing the gRNA target sites (red arrows). (b) Diagram of the AP-1 complex. (c) Immunofluorescence labeling of AP-1 γ in a mixed population of WT and μ1 KO HeLa cells. KO cells can be identified by their diffuse cytosolic labeling (arrows). Bar, 20 μm. (d) Western blots of whole-cell lysates from WT and μ1 KO HeLa cells, probed with antibodies against the μ subunit of AP-2 (which cross-reacts with the μ subunit of AP-1), clathrin heavy chain, and GGA2. AP-1 μ1 is undetectable in the μ1 KO cells, while the levels of the other coat components were unaffected by the KO. (e) Loss of μ1 causes surface accumulation of the CD8-Furin* chimera. WT and μ1 KO cells were cotransfected with CD8-Furin* and GFP-encoding plasmids and analyzed by flow cytometry (10,000 cells/cell line). GFP-positive cells were gated (left, black rectangle), and overlay histograms were plotted to calculate the mean CD8 fluorescence of the gated cells (middle). The fold change in surface CD8 was plotted as mean ± SEM (right; n = 3 repeats, KO data pulled from two independent KO clones; **, P < 0.01; Student's t test).

guished from those associated with the plasma membrane because of their different focal planes, and in both control and μ1 KO cells, we found clathrin-containing spots in the interior of the cell (Fig. 3 c).

What machinery and cargo do intracellular CCVs contain when they form in the absence of AP-1? In previous studies, we have used stable isotope labeling with amino acids in cell culture (SILAC)–based mass spectrometry to look for changes in CCV-enriched fractions when particular coat components are either depleted by siRNA (Borner et al., 2012) or rapidly removed from the available pool using our knock-sideways (KS) system (Hirst et al., 2012, 2015). The KS system was particularly informative for AP-1, enabling us to identify ∼100 CCV proteins that are depleted twofold or more from our CCV fractions (Hirst et al., 2012).

We used the same approach to compare CCV-enriched fractions from our two KO cell lines with CCV-enriched fractions from control cells. The values for selected proteins associated with intracellular CCVs are shown in Fig. 4 a (ratio of WT over KO, log₂), with the full data set (including non-CCV proteins) available in Table S1 and shown graphically in Fig. 4 b. In most cases, the changes were similar for the two KO cell lines (Fig. 4 b). Subunits of AP-1 were the most strongly depleted coat proteins (the reason μ1 has a finite number is that the control cells were grown in "heavy" medium, and not all of the protein had incorporated the heavy label), and the most strongly depleted cargo protein was CPD. Other CCV components, both machinery and cargo, were generally less affected in the KO CCVs than in our KS CCVs (Hirst et al., 2012), and some were even increased (Fig. 4 c), indicating that the cells had managed to compensate for the loss of AP-1. For instance,

three key pieces of machinery—ARF1, which is required for the formation of intracellular CCVs (Stamnes and Rothman, 1993); PI4K2B, a PI 4-kinase that contributes to AP-1 function and TGN/endosome sorting (Wieffer et al., 2013); and the alternative adaptor GGA2, which specifically sorts hydrolases and their receptors (Hirst et al., 2012)—are all strongly depleted from KS CCVs. However, ARF1 is barely affected in the μ1 KO CCVs, PI4K2B is increased, and GGA2 is unaffected in CCVs from the exon 2 cell line and increased in CCVs from the exon 4 cell line. The CCVs from the exon 4 cell line also showed a modest increase in GGA cargo, specifically the three hydrolase receptors (M6PR, IGF2R, and SORT1) and several hydrolases. Total levels of GGAs were unaffected in this cell line (Fig. 2 d), indicating that the cells had adapted to the loss of AP-1 by somehow making the GGAs work more efficiently.

Binding of μ1 to acidic clusters

The availability of μ1-null cells gave us the opportunity to test the importance of various binding sites in vivo, without any background from the endogenous protein. First, however, we wanted to test whether the electrostatic interaction between the basic patch in μ1 and the Nef acidic cluster seen in the crystal structure (Jia et al., 2012) also contributes to the recognition of endogenous acidic cluster-containing cargo proteins. This was particularly important because phosphorylation of serine and threonine residues in the acidic cluster has been shown to contribute to the sorting of proteins such as furin (Jones et al., 1995), but the Nef acidic cluster is not phosphorylated.

Our strategy was to carry out GST pulldown experiments with recombinant proteins expressed in *Escherichia coli*. As prey, we used the C-terminal MHD of μ1, incorporating a His
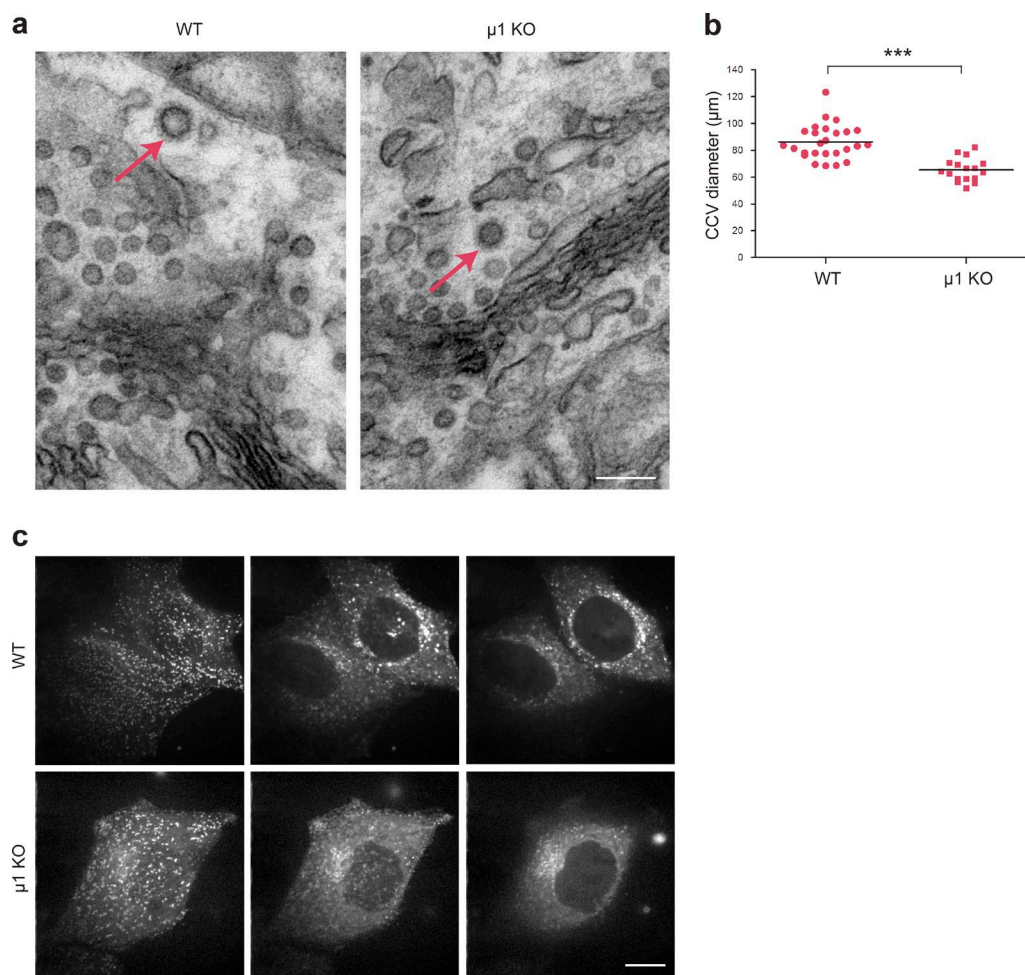
a WT   μ1 KO

b

c WT   μ1 KO

Figure 3. **Intracellular CCVs in μ1 KO cells.** (a) Electron micrographs of WT cells (left) and μ1 KO cells (right) showing clathrin-coated profiles in the TGN region (arrows). Bar, 200 nm. (b) Diameters of clathrin-coated profiles in the TGN region. The μ1 KO causes a decrease from 86 to 65 nm. Data are shown as individual symbols for each TGN-associated CCV, with bars representing the mean (*n* = 10 cells measured for each condition; ***, P < 0.001; Student's *t* test). (c) Spinning disk confocal microscopy of WT cells (top) and μ1 KO cells (bottom) expressing mCherry-tagged clathrin light chain. Three images collected at different focal planes, from the plasma membrane (left) to the perinuclear region (right), are shown for each condition. Both cell types have both plasma membrane and intracellular CCVs. Bar, 20 μm.

tag for ease of purification followed by a myc tag for anti-body labeling (Fig. 5 a). The bait was GST attached either to the MHCI-Nef chimera that was used for crystallography (Jia et al., 2012) or to the cytosolic tail of furin (Fig. 5 a). Four furin constructs were made: WT furin tail (WT), WT with serine residues phosphorylated in vitro by casein kinase 2 (Phos), an acidic cluster mutant (AC-), and a YXXΦ mutant (AKGL; Fig. 5 b). The seven recombinant proteins are shown in the Coomassie blue–stained gel in Fig. 5 c. Western blots of the pulldowns showed that the GST-MHCI-Nef and the GST-Furin-Phos constructs were most efficient at pulling down μ1 MHD. The nonphosphorylated WT furin tail bound only weakly, and the AC and AKGL mutants more weakly still, although consistently there was detectably more μ1 pulled down than with GST alone. These results indicate that the furin tail can bind to the μ1 MHD, and that phosphorylation of serine residues in the acidic cluster of the furin tail increases its affinity.

To obtain quantitative measures of these interactions, we performed isothermal titration calorimetry (ITC) experiments using furin-derived peptides (Fig. 5 b). The phosphorylated furin peptide showed very clear and reproducible

binding to μ1 with a K_D of ∼22 μM, while the nonphosphorylated version of the same peptide bound with a weaker K_D of 100–200 μM (Fig. 5 d). The binding of the phosphorylated peptide was dominated by a high enthalpic contribution of ∼16 kJ/mol, which was stronger than that observed for the nonphosphorylated peptide, suggesting a direct ionic interaction between the phosphates and the μ1 basic patch. ITC experiments with the furin peptide lacking the YKGL motif (AC only), or one in which four acidic residues were mutated to alanines (AC-), showed no measurable binding (K_D > 300 μM) to the μ1 MHD (Fig. 5 d). We also performed surface plasmon resonance (SPR) experiments, in which μ1 MHD carrying a C-terminal Avitag (Cull and Schatz, 2000) was attached to the surface of a chip coated with streptavidin and the peptides passed over it as analytes. The K_D for the phosphorylated furin peptide binding to μ1 was estimated at ∼35 μM (Fig. 5 e). We could not estimate a K_D for the non-phosphorylated furin peptide, because the binding was too weak, whereas a TGN38 peptide carrying a canonical YXXΦ signal bound with a K_D of ∼20 μM (unpublished data). Thus, all three types of experiments, pulldown, ITC, and SPR,

a

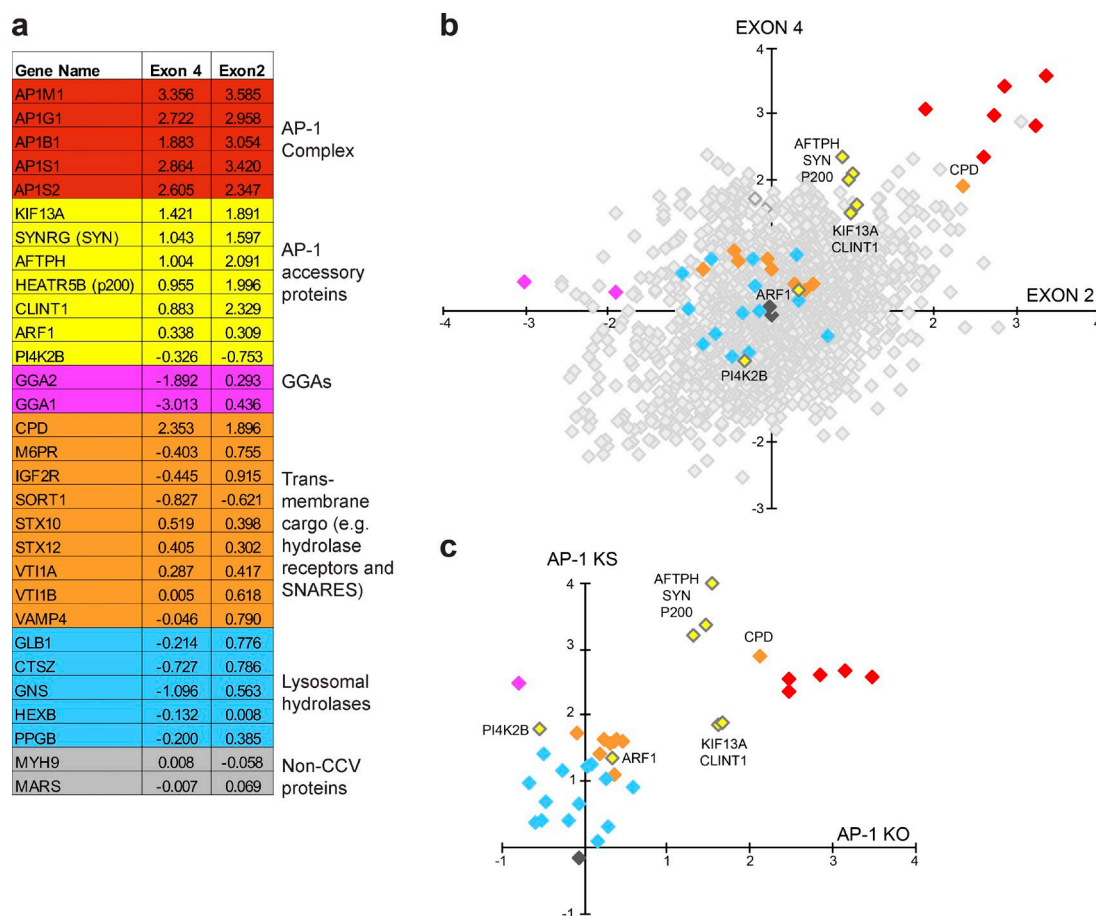| Gene Name	Exon 4	Exon2	
AP1M1	3.356	3.585	AP-1 Complex
AP1G1	2.722	2.958	
AP1B1	1.883	3.054	
AP1S1	2.864	3.420	
AP1S2	2.605	2.347	
KIF13A	1.421	1.891	AP-1 accessory proteins
SYNRG (SYN)	1.043	1.597	
AFTPH	1.004	2.091	
HEATR5B (p200)	0.955	1.996	
CLINT1	0.883	2.329	
ARF1	0.338	0.309	
PI4K2B	-0.326	-0.753	
GGA2	-1.892	0.293	GGAs
GGA1	-3.013	0.436	
CPD	2.353	1.896	Trans-membrane cargo (e.g. hydrolase receptors and SNARES)
M6PR	-0.403	0.755	
IGF2R	-0.445	0.915	
SORT1	-0.827	-0.621	
STX10	0.519	0.398	
STX12	0.405	0.302	
VTI1A	0.287	0.417	
VTI1B	0.005	0.618	
VAMP4	-0.046	0.790	
GLB1	-0.214	0.776	Lysosomal hydrolases
CTSZ	-0.727	0.786	
GNS	-1.096	0.563	
HEXB	-0.132	0.008	
PPGB	-0.200	0.385	
MYH9	0.008	-0.058	Non-CCV proteins
MARS	-0.007	0.069	

Figure 4. **CCV proteome in µ1 KO cells.** (a) CCV-enriched fractions were isolated from SILAC-labeled WT cells and two independent µ1 KO clones, made with gRNAs targeting either exon 4 or exon 2. The $\log_2$-transformed normalized ratios (WT/KO) are shown for selected AP-1–associated proteins. A positive ratio reflects depletion of a protein in the KO vesicle fraction and a negative ratio reflects enrichment. (b) The full data set of proteins (including non-CCV proteins) from each of the two experiments were plotted against each other, with the proteins in a (plus additional hydrolases) indicated in color. (c) The ratios for selected proteins from four independent KO experiments were averaged and plotted against ratios obtained from AP-1 KS experiments (Hirst et al., 2012). Some proteins (e.g., PI4K2B and GGA2) behave very differently in the KO and the KS.

showed that phosphorylation of the furin tail greatly increases its affinity for µ1.

To test the role of the basic patch more directly, we performed mutagenesis on the µ1 MHD. In addition to the basic patch, the µ1 MHD has the well-characterized "two-holed socket" which binds to YXXΦ motifs, with one pocket for the tyrosine and a second pocket for the bulky hydrophobic residue (Owen and Evans, 1998). Interestingly, in the crystal structure of the µ1–MHCI-Nef complex, the first pocket is filled by a tyrosine side chain (Y320) from MHC-I (Y320; Jia et al., 2012), explaining a long-standing paradox about why this tyrosine is essential for Nef-induced down-regulation when it is not part of a YXXΦ motif. The structure revealed that even without a bulky hydrophobic residue filling the second pocket, there are other interactions to stabilize the complex, including contacts between the Nef acidic cluster and the µ1 basic patch (Fig. 6 a). We made three µ1 mutants: a basic patch mutant, in which all five basic residues were mutated to serines (K274S, K298S, K302S, R303S, and R304S; Jia et al., 2012); a YXXΦ motif binding mutant (W408S; Farías et al., 2012); and a double mutant with both binding sites impaired. The four purified proteins are shown in the Coomassie blue–stained gel in Fig. 6 b. We performed GST pulldowns as before, using the MHCI-Nef chimera, WT furin with and without phosphorylation, and GST

alone as bait; and WT or mutant µ1 MHDs as prey. Fig. 6 c illustrates that the mutations in µ1 reduce binding, both singly and even more so in the double mutant. All three mutants were further tested for binding to the phosphorylated furin peptide by ITC and showed a clear decrease in affinity compared with the WT protein (unpublished data). However, quantification of these interactions was impossible because of the decreased mechanical stability of the mutants in the ITC cell compared with the WT protein. Similarly, we observed decreased affinity of the mutants for the phosphorylated furin peptide by SPR, while the YXXΦ-containing TGN38 peptide bound to the basic patch mutant ($K_D = \sim40$ µM) but showed no appreciable binding to the W408S mutant.

Together, these data demonstrate that µ1 is able to bind to the cytosolic tail of furin in vitro and that the same basic patch on µ1 that was shown to bind to the acidic cluster of Nef in the crystal structure (Jia et al., 2012) also contributes to the binding of a phosphorylated acidic cluster signal in an endogenous cargo protein.

Rescue of KO phenotype by WT and mutant µ1

To test the importance of the interactions between µ1 and cargo proteins in vivo, we generated stable cell lines expressing ei-
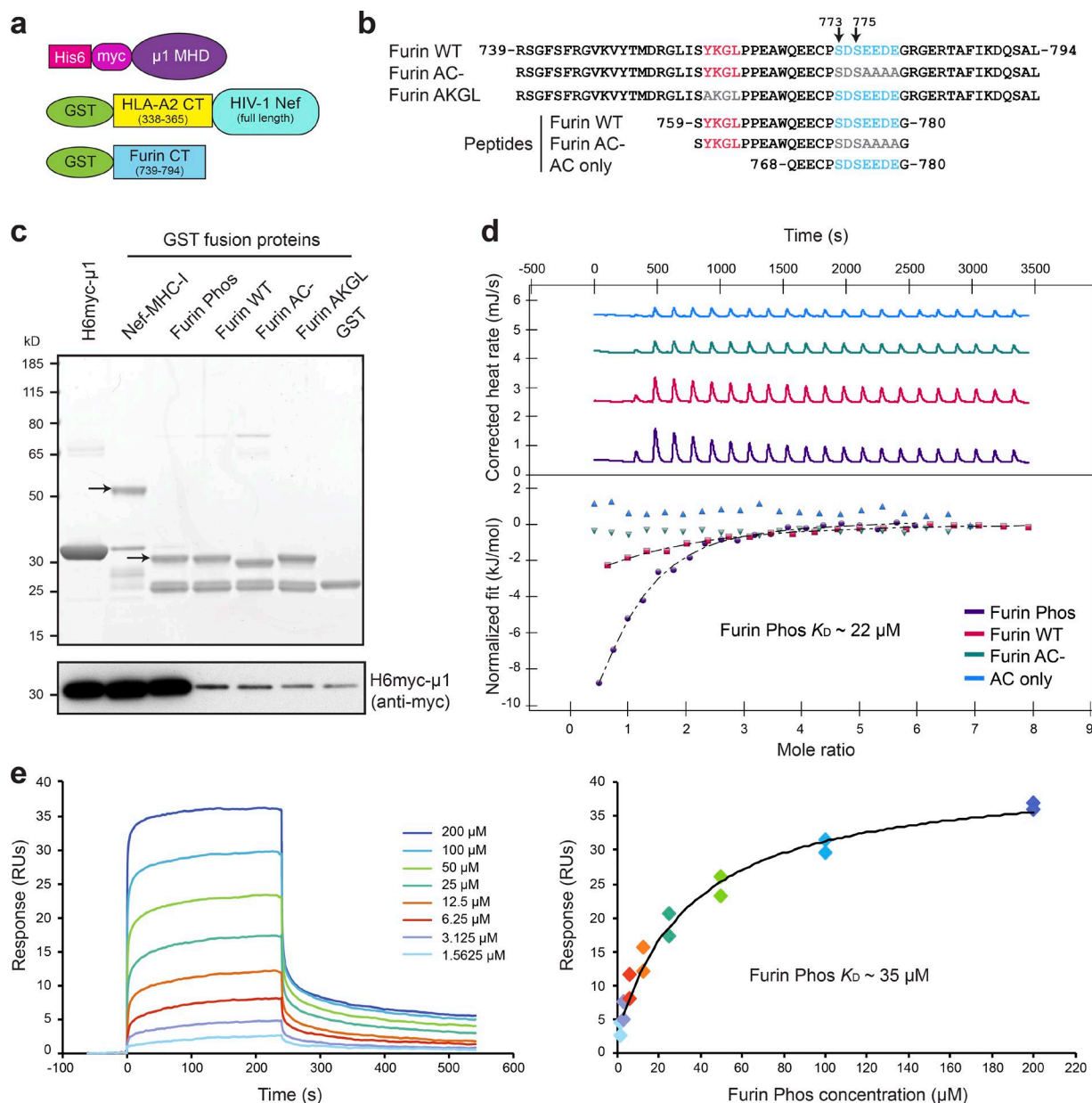
Figure 5. **Interactions between μ1 and acidic clusters.** (a) Design of the recombinant proteins. (b) Sequences of the furin cytosolic tails used in the pull-downs and synthetic peptides used for ITC and SPR. Phosphorylated serine residues marked by arrows. (c) Pulldown of WT μ1 MHD by different GST fusion proteins. (Top) Coomassie blue–stained gel of the pulldowns. Because there was some degradation of the GST constructs, arrows indicate the full-length proteins. (Bottom) Western blot of μ1 pulled down by each construct. (d) Representative ITC experiments. The μ1 MHD was titrated with four furin peptides as shown in a. The binding of μ1 MHD to the phosphorylated peptide yielding an estimate K_D of 22 ($n = 4$ independent runs). The K_D of the μ1 MHD interaction with the nonphosphorylated peptide could not be precisely calculated, because of the measurement limit of the method, but was estimated to lie between ~100 and 200 μM ($n = 6$ independent runs). (e) Representative SPR experiment. Left: sensorgrams show the response upon injection of the Furin Phos peptide onto the chip containing μ1 MHD and its dissociation. Right: response (resonance units [RUs]) at equilibrium plotted against the corresponding concentrations of Furin Phos peptide and fitted to a hyperbolic curve. Estimated K_D = ~35 μM ($n = 3$ repeats).

ther WT or mutant μ1 subunits on our exon 2 KO background. Fig. 7 a shows that all of the μ1-expressing cell lines had normal AP-1 γ labeling, indicating that all of the constructs were assembling into functional AP-1 complexes. Initially, we used flow cytometry to investigate the ability of the constructs to rescue the mislocalization of CD8-Furin* to the plasma membrane. Surprisingly, all three of the mutants rescued as well as WT μ1 (Fig. 7 b). Next we looked at a CD8 chimera with the cytosolic tail of CPD. Consistent with a previous study making use of siRNA (Harasaki et al., 2005), there was increased

surface expression of the CD8-CPD chimera in the absence of μ1. However, there was efficient rescue of the mislocalization by all four μ1 constructs. We also analyzed the distribution of two endogenous AP-1–dependent cargo proteins, CIMPR and KIAA0319L, for which there are suitable antibodies available for flow cytometry. Again, surface expression of these two endogenous proteins was increased in the μ1 KO cells, but all four μ1 constructs rescued the phenotype (Fig. 7 b).

A closer look at the cytosolic tails of the four cargo proteins showed that in every case, the tails probably contain mul-
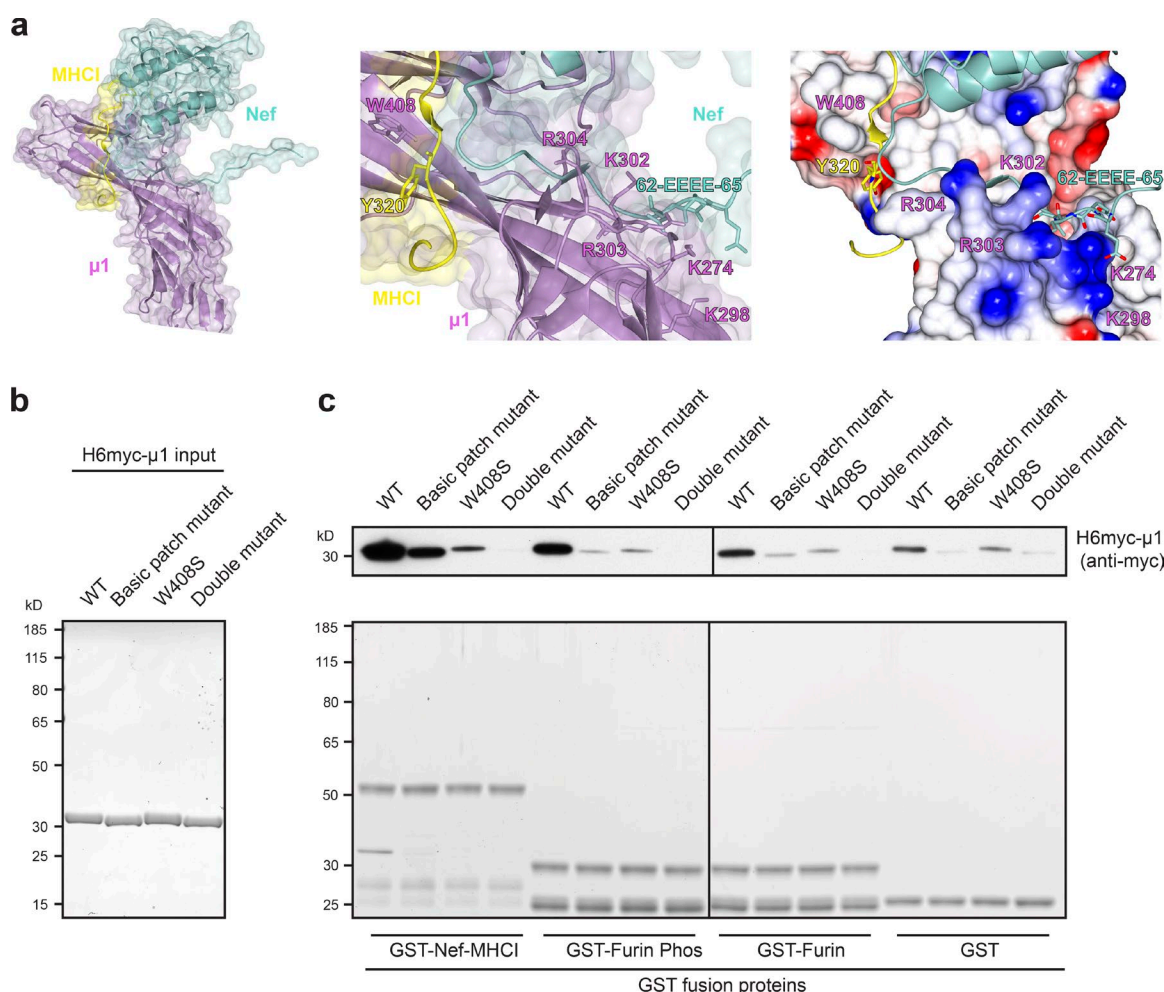
Figure 6. **Interactions between mutant μ1 and acidic clusters.** (a, left) Ribbon and molecular surface representation of the complex between Nef (cyan), the cytoplasmic domain of MHC-I (yellow), and the cargo-binding C-terminal domain of μ1 (purple; Jia et al., 2012). (Middle) Close-up of the YXXΦ and acidic cluster binding sites with key residues labeled. (Right) Key electrostatic interactions at the binding sites. Blue, positively charged; red, negatively charged. (b) Coomassie blue–stained gel of WT and mutant His6myc-tagged μ1 MHD constructs expressed in *E. coli*. (c) Pulldown of WT and mutant μ1 by four different GST constructs. (Top) Western blot of μ1 pulled down by each construct. (Bottom) Coomassie blue–stained gel of the pulldowns. The mutations introduced in μ1 compromise the binding to all of the GST constructs.

Left column:

tiple sorting motifs. Furin has not only the YXXΦ and acidic cluster motifs but also potential dileucine motifs; CPD and KIAA0319L both have YXXΦ, dileucine, and acidic cluster motifs; and CIMPR has at least four different sorting signals (Fig. 7 c). Dileucine motif–containing proteins bind to the σ1 and γ subunits rather than the μ1 subunit, and some can bind to GGAs as well. In addition, there may be other as yet unidentified sorting signals that bind to other sites on AP-1, and/or to alternative adaptors. Thus, it appears that as long as the AP-1 complex is intact, most cargo proteins are sorted even if the μ1 subunit lacks one or more binding sites.

To get a more global view of possible changes in CCV proteins in cells expressing μ1 mutants, we performed proteomics analyses of CCV-enriched fractions, using SILAC labeling to compare preparations from KO and rescued cells. Although there were differences in some of the exact ratios, probably as a result of experimental variation among preparations, all of the μ1 constructs rescued the KO phenotype, with accessory proteins and cargo showing normal incorporation into CCVs (Fig. 7 d). These results are in good agreement with our flow cytometry data, and both sets of data suggest that cells are able

Right column:

to carry out normal sorting even with mutations in the μ1 subunit, as long as the complex is able to form.

Down-regulation of MHC-I by Nef cannot be rescued by mutant μ1

Finally, we investigated the effect of the μ1 mutations on down-regulation of MHC-I by Nef. For these experiments, we made use of HeLa cells stably expressing HLA-A2, because Nef does not efficiently down-regulate the MHC-I alleles that are normally expressed by HeLa cells (Lubben et al., 2007). We repeated the KOs using the gRNAs targeting exon 2 and exon 4 and then rescued three different KO cell lines (two for exon 2 and one for exon 4) with each of the four μ1 constructs: WT μ1, basic patch mutant, W408S mutant, and double mutant. All 15 cell lines, as well as control cells, were transiently transfected with an internal ribosome entry site plasmid encoding Nef and GFP as a bicistronic message, to control for variability in expression levels (Schindler et al., 2003). The cells were shifted to 26°C after 24 h, to enhance Nef-mediated MHC-I down-regulation (Kasper et al., 2005). After a total of 48 h, they were surface-labeled for HLA-A2 and analyzed by flow cytometry.
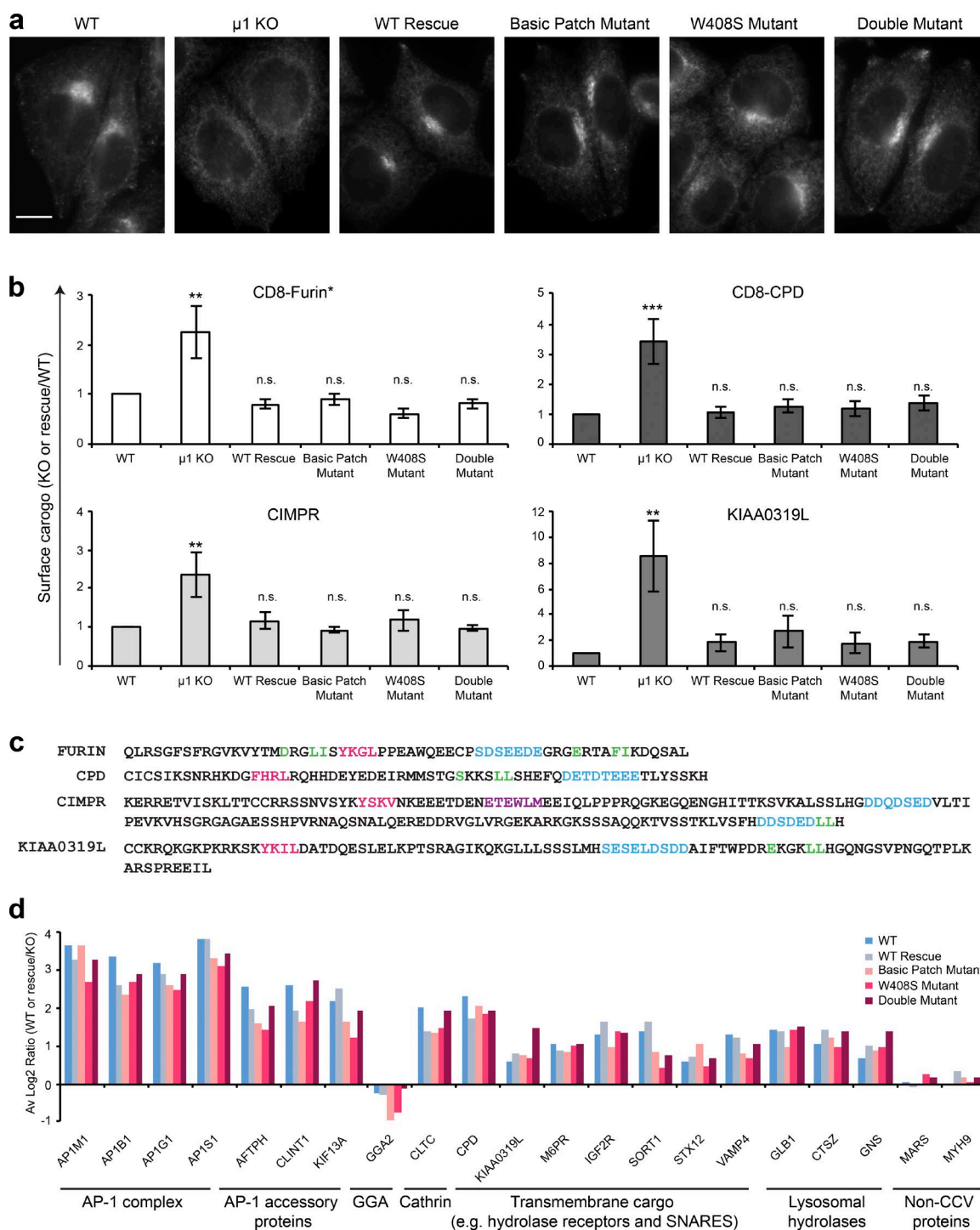
Figure 7. **Rescue of KO phenotype by WT and mutant μ1.** (a) Immunofluorescence labeling of AP-1 γ in WT cells, AP-1 μ1 KO cells, and each of the μ1 rescue cell lines. All the rescued cell lines show normal AP-1 labeling. Bar, 20 μm. (b) The six cell lines were either transfected with a CD8-Furin* plasmid or with a CD8-CPD plasmid, together with a GFP-encoding plasmid, or they were directly labeled for surface CIMPR and KIAA0319L, and surface fluorescence intensity was measured by FACS. Surface expression of all four proteins was increased in the μ1 KO cells, but all four μ1 constructs rescued the phenotype. Data represent mean fold change ± SEM (n = 3 repeats; **, P < 0.01; ***, P < 0.001; one-way ANOVA and Bonferroni post hoc test). (c) Cytosolic tail sequences of AP-1 cargo proteins with possible sorting signals highlighted in color (YXXΦ, pink; acidic cluster, blue; dileucine, green; and retromer sorting signal, purple). (d) Proteomics analysis of CCV-enriched fractions from SILAC-labeled KO and rescue cells. Abundance ratios (WT or rescue/KO) were plotted for several selected proteins. For each condition, three independent experiments were performed, once with a label swap. The normalized ratios were pooled together, log$_2$-transformed, and averaged. All of the μ1 constructs rescued the KO phenotype.

Histogram overlays are shown in Fig. 8 a comparing the surface HLA-A2 fluorescence in cells expressing moderate levels of Nef (gated for moderate GFP expression, gray) with the surface HLA-A2 fluorescence in cells not expressing Nef (GFP negative, white), for six representative cell lines. In control cells, moderate expression of Nef reduced surface HLA-A2 by 70%.
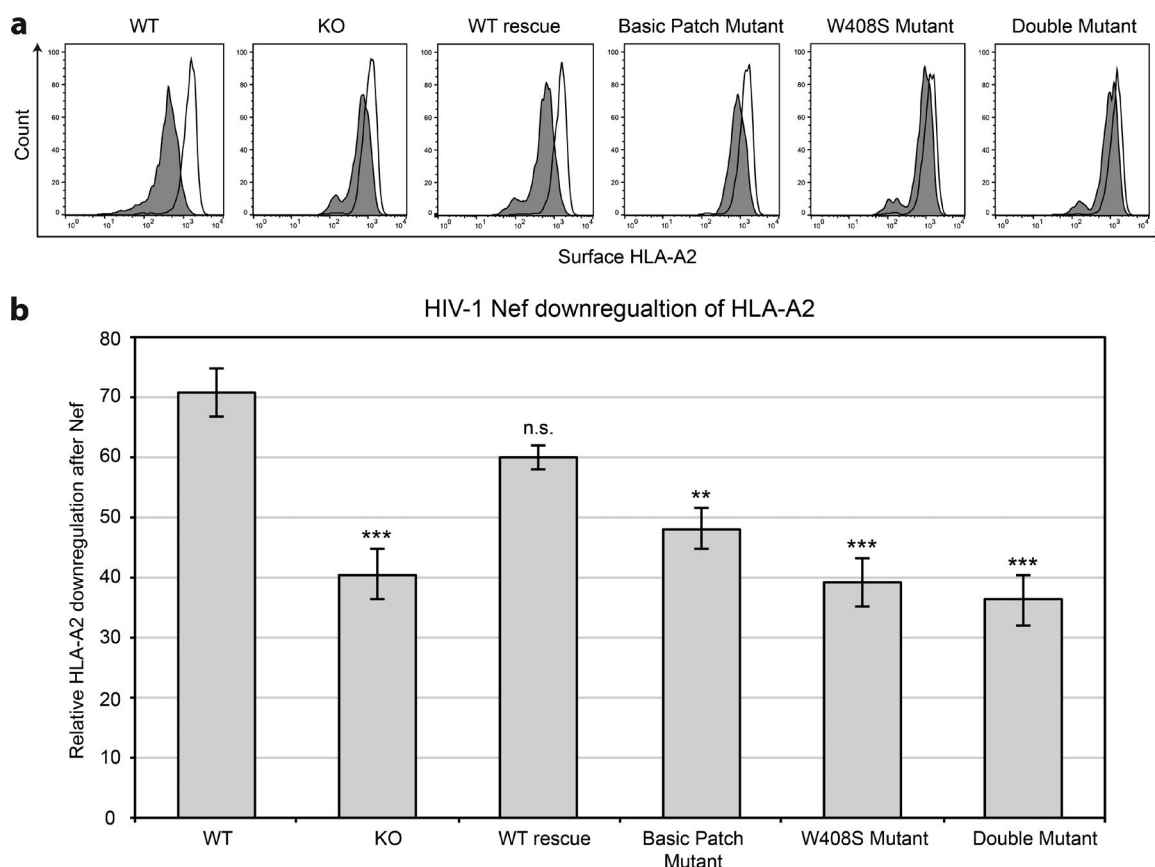
Figure 8. **Down-regulation of MHC-I by Nef cannot be rescued by mutant μ1.** WT, μ1 KO, and μ1 rescue HeLa cells stably expressing HLA-A2 were transfected with Nef-GFP on day 1, moved to 26°C on day 2, and FACS-assayed for surface HLA-A2 and GFP on day 3. (a) Histogram overlays show the surface HLA-A2 fluorescence in cells expressing moderate levels of Nef (gated for moderate GFP expression, gray) with the surface HLA-A2 fluorescence in cells not expressing Nef (GFP-negative, white), for each of the six cell lines. (b) The relative down-regulation of HLA-A2 caused by Nef was calculated as a ratio of the mean surface HLA-A2 in the presence and absence of Nef. Data represent mean ± SEM ($n = 4$ repeats; **, $P < 0.01$; ***, $P < 0.001$; one-way ANOVA and Bonferroni post hoc test). The μ1 mutants showed a definite phenotype: the basic patch mutant only partially rescued the KO phenotype, and the W408S and double mutants did not rescue the phenotype at all.

This effect was substantially reduced in the μ1 KO cells, but it was not completely abolished. Previous studies making use of siRNA to deplete AP-1 also showed inhibition but not elimination of Nef activity (Roeth et al., 2004; Lubben et al., 2007), and the present study indicates that Nef is partially functional even when AP-1 is completely absent. Adding back WT μ1 largely restored the ability of Nef to down-regulate HLA-A2. Interestingly, however, in this case the μ1 mutants did not behave like the WT protein. The basic patch mutant only partially rescued the KO phenotype, and the W408S and double mutants did not rescue the phenotype at all (Fig. 8 b). This is the first demonstration that Nef needs both the basic patch and the YXXΦ binding site on μ1 for efficient down-regulation of MHC-I in vivo.

Discussion

We have successfully used forward genetic screens in human near-haploid cells to identify machinery involved in clathrin-mediated trafficking of both YXXΦ and acidic cluster proteins. Forward genetic screens offer several advantages over siRNA screens. They are considerably faster, they are much less expensive, and off-target hits are virtually nonexistent because the only genes that are pursued are those that have been independently disrupted multiple times. Moreover, the disruptions produce a complete rather than a partial loss of a protein of interest. However, if a gene is essential for life, siRNA screens may be more informative, so the two approaches are complementary. Because we have now performed both types of screens to look for increased surface expression of CD8-YAAL, we can directly compare the hits, and there is only one in common, dynamin-2. The other eight well-characterized hits from the siRNA screen—clathrin heavy chain, the AP-2 μ subunit, and six subunits of the vacuolar ATPase (Kozik et al., 2013)—were not identified in the forward genetic screen. Interestingly, seven of these eight genes are predicted to be essential in KBM7 cells, which explains why we did not detect them (Blomen et al., 2015). In contrast, we did detect CALM, which is a known player in clathrin-mediated endocytosis, but which was not picked up in our siRNA screen. Thus, a complete removal of the protein may be necessary to get a robust effect on clathrin-mediated endocytosis.

However, the major aim of our screens was to find machinery involved in the sorting of acidic cluster-containing proteins, and here we identified two hits with increased surface expression and two with decreased surface expression. Although little is known about either of the two hits with decreased surface expression, there are reasons to believe that at least one of them, the small GTPase Rab10, is physiologically relevant. Rab10 has been implicated in the recycling of specific cargo from endo-

somes back to the plasma membrane (Sano et al., 2008; Shi et al., 2012), so loss of Rab10 may cause CD8-Furin* to accumulate in endosomes and become lost from the cell surface. In addition, a genetic interaction between Rab10 and AP-1 has been reported in *C. elegans* (Michaux et al., 2011). It is less clear why knocking out the other gene, KLHL21, would cause decreased surface expression of CD8-Furin, because all that is known about KLHL21 is that it interacts with Cullin3 to form part of an E3 ligase implicated in mitosis (Maerki et al., 2009). Further studies will be needed to find out whether it also participates in membrane traffic. One of the two hits with increased surface expression of CD8-Furin*, WDR11, is also poorly characterized. However, it was identified together with AP1M1 and other trafficking machinery in an siRNA screen for hits that sensitize cells to the toxin ricin (Bassik et al., 2013). Thus, even though WDR11 does not behave like a CCV-associated protein (Borner et al., 2014), two independent studies indicate that it contributes to the sorting of CCV cargo proteins.

Our fourth hit was the AP-1 µ1 subunit. The AP complexes always operate as heterotetramers, so one might have expected other subunits to have been identified as hits as well. However, most of the subunits are encoded by more than one gene, including µ1, for which there are two genes in mammals, but the second one (*AP1M2*) is expressed only in polarized epithelial cells (Ohno et al., 1999). In contrast, the three genes encoding the small (σ1) subunit are all expressed ubiquitously. The β1 gene is single copy; however, β1 and β2 diverged relatively recently and can substitute for each other (they are the only AP subunits that are at all promiscuous; Page and Robinson, 1995). There are also two copies of the γ gene, *AP1G1* and *AP1G2*, although little is known about *AP1G2*. Interestingly, µ1 (but not other AP-1 subunits) was also identified as a hit in a life-or-death screen performed in KBM7 cells for genes involved in cell killing by a *Pseudomonas aeruginosa* exotoxin (Tafesse et al., 2014). The authors assumed that this was because AP-1 was involved in the trafficking of the toxin, but another strong hit was furin, which processes the toxin, so AP-1 might also contribute to toxicity by localizing furin to the right compartment.

Contrary to a previous study (Meyer et al., 2000), we found that AP-1 KO cells were still able to make intracellular CCVs, but they were smaller than normal and with an altered protein content. Predictably, AP-1 itself was most strongly depleted from the CCV-enriched fraction, but there were also reductions in other machinery and cargo, in particular the acidic cluster-containing protein CPD (furin is of very low abundance in HeLa cells and was not detected in the preparation). However, some proteins were either unaffected or actually increased, including GGAs and their cargo. By comparing these results with the results of our previous study on CCVs from AP-1 KS cells (Hirst et al., 2012), we can gain some insights into how cells adapt to the loss of AP-1 in the short and long term. In the KS CCV-enriched fraction, virtually all of the proteins known to be associated with intracellular CCVs were depleted twofold or more (Hirst et al., 2012). Therefore, when AP-1 is rapidly removed from the available pool (i.e., within 10 min), the cell does not have time to adjust, and consequently it is unable to make the population of CCVs that would normally contain AP-1. In a KO, however, the cell has many days to compensate for the loss of AP-1 by up-regulating other trafficking pathways, and this ensures that most cargo reaches its appropriate destination. Getting hydrolases to the lysosome appears to be particularly important. But one cargo protein that fails to be packaged into CCVs in the µ1 KO cells is CPD, and this is further evidence that acidic cluster-containing proteins are sorted directly by AP-1.

Although it has been widely assumed that cargo proteins with acidic clusters use the same sorting machinery as Nef, up until now there has been no evidence that this is in fact the case, other than the finding that both require AP-1. All of the acidic clusters on endogenous proteins contain casein kinase II phosphorylation sites, while the Nef acidic cluster does not, suggesting that they might interact with different partners. However, we found in both our pulldowns and our biophysical assays that the phosphorylated furin tail and the MHC-I-Nef chimera bind to the µ1 C-terminal domain, and that optimal binding requires both the basic patch and the YXXΦ binding site, indicating that the molecular mechanisms for cargo recognition and Nef-induced MHC-I down-regulation are the same.

We were able to use our µ1 KO cells as a background to test the importance of these two binding sites on in vivo. Surprisingly, mutating the basic patch or the YXXΦ binding site, either alone or together, made virtually no difference to the sorting of various cargo proteins. Most of these cargo proteins are missorted to a greater or lesser degree when AP-1 is knocked out, so the explanation does not seem to be that they can use other AP complexes. Instead, the cargo proteins appear to have multiple sorting signals, so abolishing one or even two interactions has no obvious effect.

In contrast, HIV-1 Nef appears to need both of the binding sites on µ1 to down-regulate MHC-I effectively. The importance of the YXXΦ binding site had already been tested in living cells, although not in a µ1-null background (Wonderlich et al., 2008), so the inability of the W408S mutant to rescue the µ1 KO phenotype was not unexpected. However, the interaction between the acidic cluster on Nef and the basic patch on µ1 had never been tested in vivo, and without such a test, there is always the possibility that the interaction might be an artifact of crystal packing. Unlike the W408S mutant, the basic patch mutant did at least partially rescue the KO phenotype, but this is consistent with studies on Nef itself and on MHC-I. The tyrosine in MHC-I is absolutely essential for down-regulation to occur (Le Gall et al., 1998), and this agrees with our rescue data. However, mutagenesis studies have shown that neutralizing the acidic cluster on Nef impairs its ability to down-regulate MHC-I but does not completely abolish it (Williams et al., 2005; Lubben et al., 2007), and this also agrees with our rescue data. It also fits in with our in vitro binding data, where mutating the basic patch had less of an effect than mutating the YXXΦ binding site.

Why do the mutant µ1 constructs rescue the CCV cargo sorting phenotype, but not the Nef-induced down-regulation phenotype? One difference between endogenous cargo proteins and Nef is that the endogenous proteins are much more ancient. Orthologues of many of the human CCV cargo proteins are also found in CCVs from *Drosophila* S2 cells, including furin, CPD, and hydrolase receptors (Borner et al., 2014). Like the human proteins, the *Drosophila* proteins appear to have multiple sorting signals, including acidic clusters. The lineages that gave rise to insects and vertebrates are thought to have split more than 500 million years ago (Erwin and Davidson, 2002; Peterson et al., 2004), so the genes encoding these proteins must all predate that split, and the presence of multiple sorting signals must confer selective advantages. These advantages may include the availability of backup mechanisms if one sorting step fails ("belt and braces"), the ability to fine-tune the steady-state

localizations of the various proteins and the pathways they traverse, and the possibility of turning on or off one signal at a time (e.g., by phosphorylation). In contrast, Nef is a much more recent innovation, with no apparent homologues outside of primate lentiviruses, and it may not need to be very sophisticated, as long as it can do its job.

Nef down-regulates other proteins in addition to MHC-I, including the HIV-1 coreceptor CD4 and the SERINCs, which are proteins of unknown function whose presence in the virion greatly impairs infectivity (Chaudhuri et al., 2007; Usami et al., 2015). Interestingly, CD4 and SERINCs are kept off the plasma membrane by a different mechanism, which involves AP-2 rather than AP-1, specifically its dileucine binding site. Another HIV-1 regulatory protein, Vpu, also down-regulates CD4, as well as other proteins including an alanine transporter, SNAT1 (Matheson et al., 2015), and tetherin, a protein that attaches newly budded virions to the host cell plasma membrane so they cannot escape and infect other cells (Neil et al., 2008). In the case of tetherin, AP-1 has been shown to be involved. Like MHC-I, the binding of tetherin to the YXXΦ binding site of μ1 appears to be strengthened by an interaction between Vpu and the dileucine binding site of AP-1 (Neil et al., 2008). It will be important to find out whether these dileucine interactions are essential for down-regulation and also whether mutating key dileucine-binding residues in the AP-1 and AP-2 complexes inhibits down-regulation without appreciably affecting the sorting of endogenous proteins. The trend revealed by the present study suggests that even though endogenous proteins and pathogen virulence factors may make use of some of the same trafficking machinery, the endogenous proteins are much better at tolerating the disruption of single binding sites. There is a lot of interest in designing drugs that target interactions between HIV-encoded proteins and host proteins (Jäger et al., 2011; Ren et al., 2014), but the assumption has always been that these interactions must be unique to the virus, because otherwise the drugs would have unacceptable side effects. However, such interactions may be difficult to uncover, or even nonexistent. The present study indicates that in some cases, it may be possible to target highly conserved interactions that are shared by host cell proteins, and still preferentially block the function of the viral proteins.

Materials and methods

Antibodies and peptides

Antibodies used in this study include in-house antibodies against clathrin heavy chain (Hilda, rabbit; Simpson et al., 1996) and commercially available antibodies against AP-1 γ (mAb100/3, mouse; A4200; Sigma-Aldrich), AP-1 μ1 and AP-2 μ2 (AP50, mouse; 611351; BD Biosciences; although raised against μ2, this antibody cross-reacts with μ1), CIMPR (2G11, mouse; ab2733; Abcam), HLA-A2 (BB7.2, mouse; 558570; BD Biosciences), KIAA0319L (mouse; ab105385; Abcam), myc-tag (4A6, mouse; 05-724; Millipore) and Alexa Fluor 647–labeled anti-CD8 (MCA1226A647, mouse; Serotec). The mouse monoclonal antibody against GGA2 was a gift from D. Brooks (Women's and Children's Hospital, North Adelaide, Australia). HRP-labeled secondary antibodies were purchased from Sigma-Aldrich, and fluorescently labeled secondary antibodies Alexa Fluor 488–labeled donkey anti–mouse IgG (A21202), Alexa Fluor 594–labeled donkey anti–rabbit IgG (A21207), and Alexa Fluor 647–labeled goat anti–rabbit IgG (A21244) were from Invitrogen.

Synthetic peptides were obtained from Genscript. The WT furin peptides included residues 759–780 of human furin flanked by serine residues, phosphorylated at residues 773 and 775 (asterisks) or nonphosphorylated (SSYKGLPPEAWQEECP*S*D*S*EEDEGS). The acidic cluster mutant (Furin AC-) included the same residues with the mutation 776-EEDE-779 to 776-AAAA-779 (SSYKGLPPE AWQEECPSDSAAAAGS). The AC only truncated peptide included residues 768–780 (QEECPSDSEEDEG). The TGN38 peptide sequence was CKVTRRPKASDYQRL.

Constructs

CD8-YAAL-PIRES was previously generated in-house by Patrycja Kozik (Kozik et al., 2010). CD8-Furin* was obtained as a synthetic gene from GeneCust Europe. The HLA-A2-PIRES construct, the lentiviral expression vector pHRSIN-$_{PSFFV}$-GFP-$_{PPGK}$-Puro (1020), and the gene-trap retrovirus construct (pGT0-GFP-pA) were gifts from P. Lehner (University of Cambridge, Cambridge, England, UK). The CD8 and HLA-A2 constructs were cloned into the 1020 lentiviral vector with BamHI and NotI. The CD8-CPD construct was previously generated in-house (Harasaki et al., 2005) by cloning the luminal and transmembrane domains of CD8 and the cytosolic tail of CPD into pIRESNeo2 (BD Biosciences). Nef-GFP-pIRES (pCG.NL43Nef*pIRESgfp; described in Schindler et al., 2003), was a gift from P. Benaroch (Institut Curie, Paris, France). The mCherry-tagged clathrin light-chain plasmid was obtained from Addgene (pmcherry-LCa; 53972). The pIRESPuro and pEGFPN2 plasmids were from Clontech. WT and mutant AP-1 μ1 constructs were made by synthesizing three different gene-blocks (Integrated DNA Technologies). Block 1 contained the first 677 nucleotides of WT μ1. Two variants of Block 2 (nucleotides 678–1275) were synthesized containing either a WT or a mutant basic patch (K274S, K298S, K302S, R303S, and R304S). Block 1 was ligated with each Block 2 in a pQCXIH retroviral vector (Clontech) carrying hygromycin resistance using Gibson Assembly (NEB). Site-directed mutagenesis (QuikChange Lighting kit; Agilent Technologies) was used to create the W408S and the double mutant. The WT and mutant μ1 MHD (residues 158–423) were cloned into the pMW172H6Myc vector (generated in D. Owen's laboratory; Miller et al., 2007) containing N-terminal His$_6$ and myc tags using NdeI and HindIII sites. The Avitag (Cull and Schatz, 2000) was introduced at the μ1 MHD C terminus by PCR. GST was produced from the pGEX-4T-2 plasmid (GE Healthcare), and all GST-fusion proteins were constructed in this parental vector. The MHC-I-Nef fusion chimera was generated by fusing HLA-A2 residues 338–365 directly to full length HIV-1 Nef as described in Jia et al. (2012). This construct and the furin cytosolic tail sequences (residues 739–794), both WT and Y759A mutant, were cloned into pGEX-4T-2 using the BamHI and NotI sites. Site-directed mutagenesis was used to mutate the acidic cluster in the furin cytosolic tail (QuikChange Lighting kit).

Tissue culture

KBM7 cells were cultured in Iscove's modified Dulbecco's medium, human embryonic kidney (HEK) 293ET, and HeLa M cells in RPMI 1640 (all from Sigma-Aldrich). In all cases, the medium was supplemented with 10% fetal calf serum (vol/vol), 2 mM L-glutamine, 100 U/ml penicillin, and 100 µg/ml streptomycin (all from Sigma-Aldrich). Each cell line was regularly screened for absence of mycoplasma contamination by DAPI staining and treated with Micoplasma Removal Agent (MP Biomedicals).

For proteomics, cells were grown in SILAC medium (Thermo Fisher Scientific) supplemented with 10% (vol/vol) dialyzed fetal calf serum (10,000 molecular weight cut-off; Invitrogen), penicillin/streptomycin, and either "heavy" amino acids (L-arginine-13C615N4:HCl [50 mg/l] and

ʟ-lysine-13C615N2:2HCl [100 mg/l]; Cambridge Isotope Laboratories) or the equivalent "light" amino acids. Cells were grown in SILAC medium over seven doublings to achieve metabolic labeling.

Stable cell line production

Virus was produced in HEK 293ET cells as described previously (Duncan et al., 2012). Typically, HEK 293ET cells greater than 90% confluent in a six-well plate were transfected with 2 µg total DNA using Mirus TransIT-293 transfection reagent. The viral vectors plus the packaging plasmids pMD.GagPol and pMD.VSVG (retrovirus) or pCMVΔ8.91 and pMD.VSVG (lentivirus) were mixed in a ratio of 50:30:15 in 50 µl OptiMEM (Invitrogen), then mixed with 8 µl transfection reagent diluted in 200 µl OptiMEM, incubated for 20 min at RT, and added dropwise to the HEK 293ET cells growing in medium without antibiotics. The virus-containing supernatant was harvested 48 h post-transfection, filtered through a 0.45-µm filter, supplemented with 10 µg/ml hexadimethrine bromide (Polybrene; Sigma-Aldrich), and applied directly to the target cells. KBM7 cells were also centrifuged at 1,800 rpm for 45 min. After 3 h, fresh medium was added, and transgene expression was assayed 48 h later.

Haploid genetic screen

Haploid genetic screens were performed as described previously (Carette et al., 2009; Duncan et al., 2012). In brief, 10^8 KBM7 cells stably expressing CD8-YAAL or CD8-Furin* were mutagenized by transduction with a gene-trap retrovirus (pGT0-GFP-pA), grown for 7 d, and then sorted by FACS for high and low CD8 expression using a Becton Dickinson Influx cell sorter. A further sort to purify the CD8^{high} and CD8^{low} populations was performed 7 d later. Genomic DNA was extracted from the sorted populations and the retroviral integration sites mapped by splinkerette-PCR and 454 pyrosequencing as explained by Duncan et al. (2012).

CRISPR/Cas9-mediated gene disruption

The Zhang online CRISPR design tool (http://crispr.mit.edu; Hsu et al., 2013) was used to identify suitable gRNA targets in exons 2 (5′-CCGGAACTACCGTGGCGACG-3′), 3 (5′-CGACACGCACGC GTTCTTCT-3′), and 4 (5′-TGTTATCATCTACGAGCTGC-3′) of the *AP1M1* gene. Each gRNA was ordered as a pair of complementary oligonucleotides (Sigma-Aldrich) with the sequences 5′-CACCGN20-3′ and 5′-AAACN20C-3′, annealed and cloned into the BbsI site of the dual Cas9 and gRNA expression vector pX330 (Addgene). HeLa M cells were transfected with pX330 and pIRESpuro (Clontech) in a ratio of 3:1 using the TransIT-HeLaMONSTER transfection kit (Mirus Bio). Puromycin (1 µg/ml) selection was started 48 h after transfection. The efficiency of the KO was assessed in the mixed populations by Western blotting and immunofluorescence. Single-cell clones were isolated by serial dilution of the cells and tested for µ1 KO by Western blotting and immunofluorescence. The two clones selected from the exon 2 and exon 4 populations were further validated by sequencing. Genomic DNA was harvested using a High Pure PCR Template Purification kit (Roche), and PCR was used to amplify a ~500-bp region around the target sites. The PCR products were then blunt-end-cloned (Zero Blunt PCR Cloning kit; Invitrogen), and 10 (for exon 2) and 29 (for exon 4) clones were sent for Sanger sequencing with the M13_F primer (Beckman Coulter Genomics). Two frame-shifted sequences for *AP1M1* were identified in the cells where exon 2 had been disrupted, one with a single-base deletion and one with a two-base deletion: 5′-CTCATCTGCCGGAAC TACCGTGGC−ACGTGGACATGTCA,CTCATCTGCCGGAACTAC CGTGG−−ACGTGGACATGTCA-3′.

In the cells in which exon 4 had been disrupted, only one sequence was found (even after sequencing 29 independent clones),

which had an in-frame deletion of 12 nucleotides: 5′-GACAACTTT GTTATCATCTACG−−−−−−−−−−−−AGCTC-3′, removing a highly conserved four-residue sequence in the middle of an α helix, which presumably makes the protein unstable.

Flow cytometry

Approximately 10^6 cells were trypsinized when required, washed with PBS, and incubated with primary antibody for 30 min at 4°C. After the incubation, the cells were washed twice with PBS and incubated with fluorophore-conjugated secondary antibody for 30 min at 4°C. A further three washes in PBS were performed, and the samples were analyzed on a FACSCalibur instrument (BD Biosciences). Data analysis was performed using CELLQuest (Becton Dickinson) and FlowJo software (Tree Star). 10,000 live cells (identified by their forward scatter/ side scatter profile) were analyzed for each sample. When required, the cells were cotransfected with a CD8 chimera and a pEGFP-N2 plasmid in a 3:1 ratio 48 h before analysis, and the GFP fluorescence was used to gate for transfected cells. The mean intensity fluorescence was obtained as the geometric mean of the recorded/gated events and the fold change in the surface levels of the labeled protein calculated by dividing the geometric mean for each KO or rescue condition by that of WT cells for each independent experiment. The mean of three or more experiments was obtained and the SEM was calculated. Statistically significant differences were determined using a two-tailed independent-samples t test (homogeneity of variance tested with Levene's test) when only two samples were compared. Otherwise, one-way ANOVAs followed by Bonferroni post hoc tests were used.

HLA-A2 down-regulation by Nef

WT, µ1 KO, and rescue HeLa cells expressing HLA-A2 were transfected with Nef-GFP-pIRES and moved to a 26°C incubator 24 h later. The cells were labeled with anti-HLA-A2 and analyzed by flow cytometry on a FACSCalibur instrument 48 h post-transfection. Dot plots for GFP versus HLA-A2 were plotted and gates drawn around Nef-GFP negative and positive (moderate expression) populations. The HLA-A2 mean fluorescence intensity of the gated populations was used to calculate the percentage HLA-A2 down-regulation by Nef by applying this equation: $[1 − (HLA\text{-}A2\ Nef/HLA\text{-}A2\ no\ Nef) \times 100]$. The mean down-regulation achieved by Nef in two different clonal cell lines and three independent experiments was calculated. Statistically significant differences were determined using one-way ANOVA followed by a Bonferroni post hoc test.

Fluorescence microscopy

Cells grown on glass coverslips (13 mm). They were fixed at RT in 3.3% (vol/vol) paraformaldehyde in PBS and permeabilized with 0.1% Triton X-100 (Sigma-Aldrich) made up in PBS-BSA (0.5% BSA in PBS). Primary and Alexa Fluor–conjugated secondary antibodies (Alexa Fluor 488 and 594) were diluted in PBS-BSA and incubated for 45 min at RT. Each incubation was followed by at least five washes in PBS-BSA and a final three washes in PBS only. The coverslips were mounted with ProLong Gold Antifade Reagent (Thermo Fisher Scientific). Where representative images are shown, the experiment was repeated at least three times and imaging 40 fields. Where KO cell lines were used, at least two independent clones generated with different gRNAs were compared with WT cells. Wide-field fluorescent images were captured at RT with an AxioImager Z2 motorized upright microscope (63×/1.4 NA oil immersion objective; ZEISS) equipped with a and AxioCam 506 (ZEISS) and ORCA Flash 4 v2 (Hamamatsu) cameras. AxioVision and ZenBlue analysis software (ZEISS) was used for image acquisition and processing. WT and µ1 KO HeLa cells transfected with clathrin-mCherry were grown on 25-mm round coverslips and imaged at

37°C in CO₂-independent medium (Invitrogen) using a Cell Observer SD microscope equipped with a 63×/1.4 NA objective lens, a charge-coupled device camera (AxioCam MRm), and AxioVision software version 4.8 (all from ZEISS).

Electron microscopy

For conventional electron microscopy, WT and μ1 KO HeLa cells were fixed with 2% paraformaldehyde/2.5% glutaraldehyde in 0.1 M cacodylate buffer, pH 7.2, and postfixed with 1% osmium tetroxide, followed by incubation with 1% tannic acid to enhance contrast. Cells were dehydrated using increasing percentages of ethanol before being embedded onto epoxy resin (Agar Scientific) stubs. Ultrathin sections were cut using a diamond knife mounted to a Reichert Ultracut S ultramicrotome, and floating sections were collected onto copper grids. Grids were poststained with drops of lead citrate. Sections were viewed on an FEI Tecnai transmission electron microscope at a working voltage of 80 kV. The diameters of CCVs in the vicinity of the Golgi were quantified using ImageJ software (National Institutes of Health). Eight different cells were analyzed for each condition (WT or KO), and the mean size of CCVs was calculated. Statistical significance was determined with a two-tailed independent-samples t test assuming equal variances.

SDS-PAGE and immunoblotting

Cells were lysed in 2.5% (wt/vol) SDS/50mM Tris, pH 8.0. Lysates were incubated at 65°C, passed through a QIAshredder column (QIAGEN), and boiled in NuPAGE LDS sample buffer. Samples were loaded at equal protein amounts for SDS-PAGE, performed on NuPAGE 4%–12% Bis-Tris gels in NuPAGE MOPS SDS Running Buffer (Thermo Fisher Scientific). PageRuler Plus Prestained Protein Ladder (Thermo Fisher Scientific) was used to estimate the molecular size of bands. After electrophoresis using constant voltage, gels were either stained in Coomassie blue (SimplyBlue SafeStain; Thermo Fisher Scientific) or transferred to nitrocellulose membrane by wet transfer. Membranes were blocked in 5% wt/vol milk in PBS with 0.1% v/vTween-20 (PBS-T). Primary antibodies were added for at least 1 h at RT, followed by washing in PBS-T, incubation in secondary antibody for 30 min at RT, and final washes in PBS-T and PBS. Chemiluminescence detection of HRP-conjugated secondary antibody/protein-A was performed using AmershamECL Prime Western Blotting Detection Reagent (GE Healthcare) and x-ray film (Kodak). Where representative blots are shown, the experiment was repeated at least two times.

Preparation of CCV-enriched fractions

CCV-enriched fractions were prepared as described previously (Borner et al., 2006, 2012). In short, eight confluent 16-cm dishes of HeLa cells were scraped into ∼7 ml of buffer A (0.1 M MES, pH 6.5 [adjusted with NaOH], 0.2 mM EGTA, and 0.5 mM MgCl₂), homogenized with a motorized Potter-Elvehjem homogenizer, and centrifuged at 4,000 g for 32 min. The supernatant was treated with 50 μg/ml RNase A (MP Biomedicals) for 60 min at 4°C. Partially digested ribosomes were pelleted by centrifugation (4,000 g for 3 min) and discarded. Membranes were pelleted by spinning at 55,000 rpm for 40 min in a MLA-80 rotor (Beckman Coulter) and then resuspended in ∼400 μl buffer A using a 1 ml hand-held Dounce homogenizer. The suspension was mixed with an equal volume of 12.5% Ficoll/12.5% sucrose in buffer A and centrifuged in a TLA-100 rotor at 20,000 rpm for 34 min to pellet the bulk of the non-CCV membranes. The supernatant was diluted with four volumes of buffer A, and the CCVs were collected by spinning in a TLA-100 rotor at 35,000 rpm for 30 min. The final CCV-enriched pellet was resuspended in 30–50 μl of 1× sample buffer (in 2.5% SDS buffer) and

heated to 65°C for 3 min. Protein concentrations were estimated with a BCA assay (Thermo Fisher Scientific).

For binary comparisons, CCV fractions prepared from SILAC heavy and SILAC light cells were pooled (∼20–50 μg protein per fraction; equal amounts pooled). Samples were adjusted with 1:3 volumes of 4× sample buffer (10% [wt/vol] SDS, 40% [vol/vol] glycerol, 8% [vol/vol] 2-mercaptoethanol, and 200 mM Tris-HCl, pH 6.8), reduced at 90°C for 3 min, and separated in a single lane by SDS-PAGE. Gels were stained with Coomassie blue, and each lane was cut into 20 slices. Proteins were reduced, alkylated with iodoacetamide, digested in-gel using trypsin, and analyzed by LC-MSMS using a Q Exactive coupled to an RSLCnano3000 (Thermo Fisher Scientific).

Proteomics data analysis

The raw data files were processed using MaxQuant 1.3.0.5 with requantify and match between runs features enabled. The primary output for each SILAC comparison of CCVs was a list of identified proteins, a ratio of relative abundance (heavy/light ratio), and the number of quantification events (count). Each MaxQuant output file was formatted in an identical manner: reverse hits, proteins identified only by site, common contaminants, and proteins with no gene name were removed. Proteins with (non-normalized) ratios >50 or <0.02 were removed, as these were outside the theoretical range that could be observed with a SILAC labeling efficiency of <98%. In the case of duplicate entries for the same protein, the entry with the smaller number of quantification events was deleted. Ratios were normalized by dividing each heavy/light ratio by the median of all the heavy/light ratios for each experiment, and the ratios for the label swap experiment were inverted. The normalized ratios were log₂-transformed and the data sets for all three independent experiments pooled together and averaged. This produced a list of protein ratios identified in all experiments. The list was plotted entirely in scatterplots to compare two repeats of the same experiment, or the ratios for selected proteins of interests were plotted together in a column graph to compare the ability of the different μ1 constructs to rescue the KO phenotype.

Protein expression and purification

All recombinant proteins were expressed in BL21(DE3) pLysS cells for 16 h at 22°C after induction with 0.2 mM IPTG. Cells were lysed and insoluble material removed by centrifugation. GST fusion proteins were bound to glutathione-Sepharose 4B in 10 mM Tris-HCl, pH 7.4, 200 mM NaCl, 4 mM DTT, and 0.1 mM ABESF and were eluted with buffer containing 30 mM glutathione. N-terminally His₆- and Myc-tagged μ1 MHD (residues 158–423) was purified on Ni²⁺-NTA agarose beads in buffer A (10 mM Tris-HCl, pH 7.4, 500 mM NaCl, 1 mM β-mercaptoethanol, and 0.1 mM ABESF) and eluted in the same buffer containing 300 mM imidazole. μ1 MHD proteins were purified on a HiLoad 26/600 Superdex S200 gel filtration column (GE Healthcare) equilibrated in buffer A. For ITC, the buffer was exchanged using a PD-10 column (GE Healthcare) into 100 mM Tris-HCl, pH 7.4, 200 mM NaCl and 0.25 mM TCEP.

GST pull-down assays

GST or GST fusion protein (30–50 μg) was diluted in cold assay buffer composed of 10 mM Tris-HCl, pH 7.4, 200 mM NaCl, 0.1% NP-40, and 2 mM DTT up to a final volume of 400 μl. Cold 50% glutathione-Sepharose bead slurry in assay buffer (60 μl) was then added to each tube. After incubation at 4°C with continuous mixing for 30 min, the Sepharose beads were washed three times with 1 ml of cold assay buffer (500 g, 1 min, 4°C). After the third spin, the buffer was carefully aspirated and was replaced with 90 μg of H6mycμ1 protein diluted into 300 μl of assay buffer. After incubation at 4°C for 60 min with constant mixing, the supernatants were removed, and the beads were washed

three times in 0.5 ml of assay buffer and one final time in 1 ml of buffer (500 g, 1 min, 4°C). The bound proteins were eluted from the beads by mixing at 95°C for 5 min in reducing SDS sample buffer (2×) and were analyzed by SDS-PAGE and Western blotting with anti-Myc antibody followed by rabbit anti-mouse HRP. All pulldowns were repeated at least three times to account for reproducibility.

The GST-Furin WT fusion protein was phosphorylated using casein kinase II (P6010; NEB) following the manufacturer's instructions. The extent of phosphorylation was confirmed by mass spectrometry. The GST-Furin phosphorylated sample was digested with trypsin in solution, and the resulting peptides were analyzed using a Q Exactive coupled to an RSLCnano3000 (Thermo Fisher Scientific). Raw files were processed in Proteome Discoverer 1.4 and searched against a Uniprot Human database (downloaded August 11, 2016) using MASCOT version 2.4 with oxidized methionine and phosphorylated serine/threonine set as variable modifications. Peptides were filtered to high confidence using Percolator, and Precursor Ions Area Detector node was enabled. On the basis of the peptide peak areas, 99.8% of furin peptides were phosphorylated: 68% on both Ser773 and Ser775 and 31.8% on Ser773 only.

ITC

All ITC experiments were performed in buffer containing 200 mM NaCl, 100 mM Tris-HCl, pH 7.4, and 0.25 mM TCEP at 12°C. The synthetic peptides were dissolved in the same buffer. Experiments were performed using a Nano ITC microcalorimeter (TA Instruments). The μ1 MHD at concentrations ∼0.03–0.1 mM was placed in the cell at 12°C, and peptides (1 mM) were titrated in 20 2.4-μl injections separated by 2.5 min, preceded by a single 1.0-μl mock injection. An appropriate peptide into buffer blank was subtracted from all data runs, and for constructs that displayed measurable binding, a minimum of four independent runs that showed clear saturation of binding were used to calculate the mean K_D of the reaction, its stoichiometry (n), and their corresponding thermodynamic values. Analysis of results and final figure preparation were performed using the NanoAnalyze software.

SPR

Experiments were performed on a Biacore T200 (GE Healthcare). First, streptavidin recombinant protein (pro-791; Generon) was coupled in PBS buffer to Series S CM5 Sensor Chips (BR-1005-30; GE Healthcare) by the amine coupling protocol specified in Biacore T200 Control Software with reagents purchased from GE Healthcare. In brief, after the sensor surfaces were activated by applying a 1:1 mixture of 50 mM N-hydroxysuccinimide: 200 mM 1-ethyl-3-(3-dimethylaminopropyl) carbodiimide hydrochloride provided in the Biacore Amine Coupling kit (BR-1000-50; GE Healthcare), the streptavidin was diluted to 0.4 mg/ml in 10 mM sodium acetate, pH 4.0 (BR-1003-49; GE Healthcare), and injected into all flow cells at 5 μl/min, until ∼1,200 resonance units of protein was immobilized. 1 M ethanolamine, pH 8.5, was then injected to block remaining active sites on all four flow cells. Next, Avi-tagged GFP (flow cell 1) or C-terminally Avi-tagged μ1 (WT: flow cell 2; basic patch mutant: flow cell 3; W408S mutant: flow cell 4) were injected in the gel filtration buffer (500 mM NaCl, 10 mM Tris, pH 7.4, and 1 mM DTT). Saturated binding resulted in an observed increase of ∼1,800 resonance units in each flow cell. The binding analysis was performed at 12°C in 200 mM NaCl, 10 mM Tris, pH 7.4, and 1 mM DTT. No binding was observed in the presence of 0.5M NaCl. Peptides between 200 and 1.56 μM concentration for the furin peptides, and 50–0.195 μM for the TGN38 peptide, were injected at 30 μl/min for 240 s, followed by 300-s wash. Between each sample injection, the chip was regenerated by injecting 2.6 M NaCl, 5 mM Tris, pH 7.4, and 0.5 mM DTT at 30 μl/min for 20 s, waiting 300 s for the baseline to stabilize. Sensorgrams were processed with Biacore T200 Evaluation Software version 2.0.1 (GE Healthcare). Equilibrium dissociation constants (K_D) for binding were determined from the best fit curves to the equation for a single binding site between μ1 and peptide.

Online supplemental material

Table S1 is a complete data set comparing CCV-enriched fractions from control and KO cells.

References

Bankaitis, V.A., L.M. Johnson, and S.D. Emr. 1986. Isolation of yeast mutants defective in protein targeting to the vacuole. *Proc. Natl. Acad. Sci. USA.* 83:9075–9079. http://dx.doi.org/10.1073/pnas.83.23.9075

Bassik, M.C., M. Kampmann, R.J. Lebbink, S. Wang, M.Y. Hein, I. Poser, J. Weibezahn, M.A. Horlbeck, S. Chen, M. Mann, et al. 2013. A systematic mammalian genetic interaction map reveals pathways underlying ricin susceptibility. *Cell.* 152:909–922. http://dx.doi.org/10.1016/j.cell.2013.01.030

Baugh, L.L., J.V. Garcia, and J.L. Foster. 2008. Functional characterization of the human immunodeficiency virus type 1 Nef acidic domain. *J. Virol.* 82:9657–9667. http://dx.doi.org/10.1128/JVI.00107-08

Blomen, V.A., P. Májek, L.T. Jae, J.W. Bigenzahn, J. Nieuwenhuis, J. Staring, R. Sacco, F.R. van Diemen, N. Olk, A. Stukalov, et al. 2015. Gene essentiality and synthetic lethality in haploid human cells. *Science.* 350:1092–1096. http://dx.doi.org/10.1126/science.aac7557

Bonifacino, J.S., and L.M. Traub. 2003. Signals for sorting of transmembrane proteins to endosomes and lysosomes. *Annu. Rev. Biochem.* 72:395–447. http://dx.doi.org/10.1146/annurev.biochem.72.121801.161800

Borner, G.H.H., M. Harbour, S. Hester, K.S. Lilley, and M.S. Robinson. 2006. Comparative proteomics of clathrin-coated vesicles. *J. Cell Biol.* 175:571–578. http://dx.doi.org/10.1083/jcb.200607164

Borner, G.H.H., R. Antrobus, J. Hirst, G.S. Bhumbra, P. Kozik, L.P. Jackson, D.A. Sahlender, and M.S. Robinson. 2012. Multivariate proteomic

profiling identifies novel accessory proteins of coated vesicles. *J. Cell Biol.* 197:141–160. http://dx.doi.org/10.1083/jcb.201111049

Borner, G.H.H., M.Y. Hein, J. Hirst, J.R. Edgar, M. Mann, and M.S. Robinson. 2014. Fractionation profiling: a fast and versatile approach for mapping vesicle proteomes and protein-protein interactions. *Mol. Biol. Cell.* 25:3178–3194. http://dx.doi.org/10.1091/mbc.E14-07-1198

Carette, J.E., C.P. Guimaraes, M. Varadarajan, A.S. Park, I. Wuethrich, A. Godarova, M. Kotecki, B.H. Cochran, E. Spooner, H.L. Ploegh, and T.R. Brummelkamp. 2009. Haploid genetic screens in human cells identify host factors used by pathogens. *Science.* 326:1231–1235. http://dx.doi.org/10.1126/science.1178955

Carette, J.E., M. Raaben, A.C. Wong, A.S. Herbert, G. Obernosterer, N. Mulherkar, A.I. Kuehne, P.J. Kranzusch, A.M. Griffin, G. Ruthel, et al. 2011. Ebola virus entry requires the cholesterol transporter Niemann-Pick C1. *Nature.* 477:340–343. http://dx.doi.org/10.1038/nature10348

Chaudhuri, R., O.W. Lindwasser, W.J. Smith, J.H. Hurley, and J.S. Bonifacino. 2007. Downregulation of CD4 by human immunodeficiency virus type 1 Nef is dependent on clathrin and involves direct interaction of Nef with the AP2 clathrin adaptor. *J. Virol.* 81:3877–3890. http://dx.doi.org/10.1128/JVI.02725-06

Chen, H.J., J. Yuan, and P. Lobel. 1997. Systematic mutational analysis of the cation-independent mannose 6-phosphate/insulin-like growth factor II receptor cytoplasmic domain. An acidic cluster containing a key aspartate is important for function in lysosomal enzyme sorting. *J. Biol. Chem.* 272:7003–7012. http://dx.doi.org/10.1074/jbc.272.11.7003

Crump, C.M., Y. Xiang, L. Thomas, F. Gu, C. Austin, S.A. Tooze, and G. Thomas. 2001. PACS-1 binding to adaptors is required for acidic cluster motif-mediated protein traffic. *EMBO J.* 20:2191–2201. http://dx.doi.org/10.1093/emboj/20.9.2191

Cull, M.G., and P.J. Schatz. 2000. Biotinylation of proteins in vivo and in vitro using small peptide tags. *Methods Enzymol.* 326:430–440. http://dx.doi.org/10.1016/S0076-6879(00)26068-0

Duncan, L.M., R.T. Timms, E. Zavodszky, F. Cano, G. Dougan, F. Randow, and P.J. Lehner. 2012. Fluorescence-based phenotypic selection allows forward genetic screens in haploid human cells. *PLoS One.* 7:e39651. http://dx.doi.org/10.1371/journal.pone.0039651

Eng, F.J., O. Varlamov, and L.D. Fricker. 1999. Sequences within the cytoplasmic domain of gp180/carboxypeptidase D mediate localization to the trans-Golgi network. *Mol. Biol. Cell.* 10:35–46. http://dx.doi.org/10.1091/mbc.10.1.35

Erwin, D.H., and E.H. Davidson. 2002. The last common bilaterian ancestor. *Development.* 129:3021–3032.

Farías, G.G., L. Cuitino, X. Guo, X. Ren, M. Jarnik, R. Mattera, and J.S. Bonifacino. 2012. Signal-mediated, AP-1/clathrin-dependent sorting of transmembrane receptors to the somatodendritic domain of hippocampal neurons. *Neuron.* 75:810–823. http://dx.doi.org/10.1016/j.neuron.2012.07.007

Fölsch, H., M. Pypaert, P. Schu, and I. Mellman. 2001. Distribution and function of AP-1 clathrin adaptor complexes in polarized epithelial cells. *J. Cell Biol.* 152:595–606. http://dx.doi.org/10.1083/jcb.152.3.595

Greenberg, M.E., A.J. Iafrate, and J. Skowronski. 1998. The SH3 domain-binding surface and an acidic motif in HIV-1 Nef regulate trafficking of class I MHC complexes. *EMBO J.* 17:2777–2789. http://dx.doi.org/10.1093/emboj/17.10.2777

Guimaraes, C.P., J.E. Carette, M. Varadarajan, J. Antos, M.W. Popp, E. Spooner, T.R. Brummelkamp, and H.L. Ploegh. 2011. Identification of host cell factors required for intoxication through use of modified cholera toxin. *J. Cell Biol.* 195:751–764. http://dx.doi.org/10.1083/jcb.201108103

Harasaki, K., N.B. Lubben, M. Harbour, M.J. Taylor, and M.S. Robinson. 2005. Sorting of major cargo glycoproteins into clathrin-coated vesicles. *Traffic.* 6:1014–1026. http://dx.doi.org/10.1111/j.1600-0854.2005.00341.x

Hirst, J., G.H.H. Borner, R. Antrobus, A.A. Peden, N.A. Hodson, D.A. Sahlender, and M.S. Robinson. 2012. Distinct and overlapping roles for AP-1 and GGAs revealed by the "knocksideways" system. *Curr. Biol.* 22:1711–1716. http://dx.doi.org/10.1016/j.cub.2012.07.012

Hirst, J., J.R. Edgar, G.H.H. Borner, S. Li, D.A. Sahlender, R. Antrobus, and M.S. Robinson. 2015. Contributions of epsinR and gadkin to clathrin-mediated intracellular trafficking. *Mol. Biol. Cell.* 26:3085–3103. http://dx.doi.org/10.1091/mbc.E15-04-0245

Hsu, P.D., D.A. Scott, J.A. Weinstein, F.A. Ran, S. Konermann, V. Agarwala, Y. Li, E.J. Fine, X. Wu, O. Shalem, et al. 2013. DNA targeting specificity of RNA-guided Cas9 nucleases. *Nat. Biotechnol.* 31:827–832. http://dx.doi.org/10.1038/nbt.2647

Jäger, S., P. Cimermancic, N. Gulbahce, J.R. Johnson, K.E. McGovern, S.C. Clarke, M. Shales, G. Mercenne, L. Pache, K. Li, et al. 2011. Global landscape of HIV-human protein complexes. *Nature.* 481:365–370.

Jia, X., R. Singh, S. Homann, H. Yang, J. Guatelli, and Y. Xiong. 2012. Structural basis of evasion of cellular adaptive immunity by HIV-1 Nef. *Nat. Struct. Mol. Biol.* 19:701–706. http://dx.doi.org/10.1038/nsmb.2328

Jones, B.G., L. Thomas, S.S. Molloy, C.D. Thulin, M.D. Fry, K.A. Walsh, and G. Thomas. 1995. Intracellular trafficking of furin is modulated by the phosphorylation state of a casein kinase II site in its cytoplasmic tail. *EMBO J.* 14:5869–5883.

Kasper, M.R., J.F. Roeth, M. Williams, T.M. Filzen, R.I. Fleis, and K.L. Collins. 2005. HIV-1 Nef disrupts antigen presentation early in the secretory pathway. *J. Biol. Chem.* 280:12840–12848. http://dx.doi.org/10.1074/jbc.M413538200

Kozik, P., R.W. Francis, M.N.J. Seaman, and M.S. Robinson. 2010. A screen for endocytic motifs. *Traffic.* 11:843–855. http://dx.doi.org/10.1111/j.1600-0854.2010.01056.x

Kozik, P., N.A. Hodson, D.A. Sahlender, N. Simecek, C. Soromani, J. Wu, L.M. Collinson, and M.S. Robinson. 2013. A human genome-wide screen for regulators of clathrin-coated vesicle formation reveals an unexpected role for the V-ATPase. *Nat. Cell Biol.* 15:50–60. http://dx.doi.org/10.1038/ncb2652

Le Gall, S., L. Erdtmann, S. Benichou, C. Berlioz-Torrent, L. Liu, R. Benarous, J.M. Heard, and O. Schwartz. 1998. Nef interacts with the mu subunit of clathrin adaptor complexes and reveals a cryptic sorting signal in MHC I molecules. *Immunity.* 8:483–495. http://dx.doi.org/10.1016/S1074-7613(00)80553-1

Lubben, N.B., D.A. Sahlender, A.M. Motley, P.J. Lehner, P. Benaroch, and M.S. Robinson. 2007. HIV-1 Nef-induced down-regulation of MHC class I requires AP-1 and clathrin but not PACS-1 and is impeded by AP-2. *Mol. Biol. Cell.* 18:3351–3365. http://dx.doi.org/10.1091/mbc.E07-03-0218

Maerki, S., M.H. Olma, T. Staubli, P. Steigemann, D.W. Gerlich, M. Quadroni, I. Sumara, and M. Peter. 2009. The Cul3-KLHL21 E3 ubiquitin ligase targets aurora B to midzone microtubules in anaphase and is required for cytokinesis. *J. Cell Biol.* 187:791–800. http://dx.doi.org/10.1083/jcb.200906117

Matheson, N.J., J. Sumner, K. Wals, R. Rapiteanu, M.P. Weekes, R. Vigan, J. Weinelt, M. Schindler, R. Antrobus, A.S. Costa, et al. 2015. Cell surface proteomic map of HIV infection reveals antagonism of amino acid metabolism by Vpu and Nef. *Cell Host Microbe.* 18:409–423. http://dx.doi.org/10.1016/j.chom.2015.09.003

Meyer, C., D. Zizioli, S. Lausmann, E.L. Eskelinen, J. Hamann, P. Saftig, K. von Figura, and P. Schu. 2000. mu1A-adaptin-deficient mice: lethality, loss of AP-1 binding and rerouting of mannose 6-phosphate receptors. *EMBO J.* 19:2193–2203. http://dx.doi.org/10.1093/emboj/19.10.2193

Meyer, C., E.L. Eskelinen, M.R. Guruprasad, K. von Figura, and P. Schu. 2001. Mu 1A deficiency induces a profound increase in MPR300/IGF-II receptor internalization rate. *J. Cell Sci.* 114:4469–4476.

Michaux, G., C.E. Dyer, T.D. Nightingale, E. Gallaud, S. Nurrish, and D.F. Cutler. 2011. A role for Rab10 in von Willebrand factor release discovered by an AP-1 interactor screen in C. elegans. *J. Thromb. Haemost.* 9:392–401. http://dx.doi.org/10.1111/j.1538-7836.2010.04138.x

Miller, S.E., B.M. Collins, A.J. McCoy, M.S. Robinson, and D.J. Owen. 2007. A SNARE-adaptor interaction is a new mode of cargo recognition in clathrin-coated vesicles. *Nature.* 450:570–574. http://dx.doi.org/10.1038/nature06353

Miller, S.E., S. Mathiasen, N.A. Bright, F. Pierre, B.T. Kelly, N. Kladt, A. Schauss, C.J. Merrifield, D. Stamou, S. Höning, and D.J. Owen. 2015. CALM regulates clathrin-coated vesicle size and maturation by directly sensing and driving membrane curvature. *Dev. Cell.* 33:163–175. http://dx.doi.org/10.1016/j.devcel.2015.03.002

Motley, A., N.A. Bright, M.N.J. Seaman, and M.S. Robinson. 2003. Clathrin-mediated endocytosis in AP-2-depleted cells. *J. Cell Biol.* 162:909–918. http://dx.doi.org/10.1083/jcb.200305145

Neil, S.J., T. Zang, and P.D. Bieniasz. 2008. Tetherin inhibits retrovirus release and is antagonized by HIV-1 Vpu. *Nature.* 451:425–430. http://dx.doi.org/10.1038/nature06553

Ohno, H., T. Tomemori, F. Nakatsu, Y. Okazaki, R.C. Aguilar, H. Foelsch, I. Mellman, T. Saito, T. Shirasawa, and J.S. Bonifacino. 1999. Mu1B, a novel adaptor medium chain expressed in polarized epithelial cells. *FEBS Lett.* 449:215–220. http://dx.doi.org/10.1016/S0014-5793(99)00432-9

Owen, D.J., and P.R. Evans. 1998. A structural explanation for the recognition of tyrosine-based endocytotic signals. *Science.* 282:1327–1332. http://dx.doi.org/10.1126/science.282.5392.1327

Page, L.J., and M.S. Robinson. 1995. Targeting signals and subunit interactions in coated vesicle adaptor complexes. *J. Cell Biol.* 131:619–630. http://dx.doi.org/10.1083/jcb.131.3.619

Peden, A.A., R.E. Rudge, W.W. Lui, and M.S. Robinson. 2002. Assembly and function of AP-3 complexes in cells expressing mutant subunits. *J. Cell Biol.* 156:327–336. http://dx.doi.org/10.1083/jcb.200107140

Peterson, K.J., J.B. Lyons, K.S. Nowak, C.M. Takacs, M.J. Wargo, and M.A. McPeek. 2004. Estimating metazoan divergence times with a molecular clock. *Proc. Natl. Acad. Sci. USA*. 101:6536–6541. http://dx.doi.org/10.1073/pnas.0401670101

Ren, X., S.Y. Park, J.S. Bonifacino, and J.H. Hurley. 2014. How HIV-1 Nef hijacks the AP-2 clathrin adaptor to downregulate CD4. *eLife*. 3:e01754. http://dx.doi.org/10.7554/eLife.01754

Robinson, M.S. 2015. Forty years of clathrin-coated vesicles. *Traffic*. 16:1210–1238. http://dx.doi.org/10.1111/tra.12335

Robinson, J.S., D.J. Klionsky, L.M. Banta, and S.D. Emr. 1988. Protein sorting in Saccharomyces cerevisiae: isolation of mutants defective in the delivery and processing of multiple vacuolar hydrolases. *Mol. Cell. Biol.* 8:4936–4948. http://dx.doi.org/10.1128/MCB.8.11.4936

Roeth, J.F., M. Williams, M.R. Kasper, T.M. Filzen, and K.L. Collins. 2004. HIV-1 Nef disrupts MHC-I trafficking by recruiting AP-1 to the MHC-I cytoplasmic tail. *J. Cell Biol.* 167:903–913. http://dx.doi.org/10.1083/jcb.200407031

Sano, H., W.G. Roach, G.R. Peck, M. Fukuda, and G.E. Lienhard. 2008. Rab10 in insulin-stimulated GLUT4 translocation. *Biochem. J.* 411:89–95. http://dx.doi.org/10.1042/BJ20071318

Schindler, M., S. Würfl, P. Benaroch, T.C. Greenough, R. Daniels, P. Easterbrook, M. Brenner, J. Münch, and F. Kirchhoff. 2003. Down-modulation of mature major histocompatibility complex class II and up-regulation of invariant chain cell surface expression are well-conserved functions of human and simian immunodeficiency virus nef alleles. *J. Virol.* 77:10548–10556. http://dx.doi.org/10.1128/JVI.77.19.10548-10556.2003

Shen, Q.T., X. Ren, R. Zhang, I.H. Lee, and J.H. Hurley. 2015. HIV-1 Nef hijacks clathrin coats by stabilizing AP-1:Arf1 polygons. *Science*. 350:aac5137. http://dx.doi.org/10.1126/science.aac5137

Shi, A., O. Liu, S. Koenig, R. Banerjee, C.C. Chen, S. Eimer, and B.D. Grant. 2012. RAB-10-GTPase-mediated regulation of endosomal phosphatidylinositol-4,5-bisphosphate. *Proc. Natl. Acad. Sci. USA*. 109:E2306–E2315. http://dx.doi.org/10.1073/pnas.1205278109

Simpson, F., N.A. Bright, M.A. West, L.S. Newman, R.B. Darnell, and M.S. Robinson. 1996. A novel adaptor-related protein complex. *J. Cell Biol.* 133:749–760. http://dx.doi.org/10.1083/jcb.133.4.749

Stamnes, M.A., and J.E. Rothman. 1993. The binding of AP-1 clathrin adaptor particles to Golgi membranes requires ADP-ribosylation factor, a small GTP-binding protein. *Cell*. 73:999–1005. http://dx.doi.org/10.1016/0092-8674(93)90277-W

Tafesse, F.G., C.P. Guimaraes, T. Maruyama, J.E. Carette, S. Lory, T.R. Brummelkamp, and H.L. Ploegh. 2014. GPR107, a G-protein-coupled receptor essential for intoxication by *Pseudomonas aeruginosa* exotoxin A, localizes to the Golgi and is cleaved by furin. *J. Biol. Chem.* 289:24005–24018. http://dx.doi.org/10.1074/jbc.M114.589275

Usami, Y., Y. Wu, and H.G. Göttlinger. 2015. SERINC3 and SERINC5 restrict HIV-1 infectivity and are counteracted by Nef. *Nature*. 526:218–223. http://dx.doi.org/10.1038/nature15400

Voorhees, P., E. Deignan, E. van Donselaar, J. Humphrey, M.S. Marks, P.J. Peters, and J.S. Bonifacino. 1995. An acidic sequence within the cytoplasmic domain of furin functions as a determinant of trans-Golgi network localization and internalization from the cell surface. *EMBO J.* 14:4961–4975.

Wan, L., S.S. Molloy, L. Thomas, G. Liu, Y. Xiang, S.L. Rybak, and G. Thomas. 1998. PACS-1 defines a novel gene family of cytosolic sorting proteins required for trans-Golgi network localization. *Cell*. 94:205–216. http://dx.doi.org/10.1016/S0092-8674(00)81420-8

Wieffer, M., E. Cibrián Uhalte, Y. Posor, C. Otten, K. Branz, I. Schütz, J. Mössinger, P. Schu, S. Abdelilah-Seyfried, M. Krauß, and V. Haucke. 2013. PI4K2β/AP-1-based TGN-endosomal sorting regulates Wnt signaling. *Curr. Biol.* 23:2185–2190. http://dx.doi.org/10.1016/j.cub.2013.09.017

Williams, M., J.F. Roeth, M.R. Kasper, T.M. Filzen, and K.L. Collins. 2005. Human immunodeficiency virus type 1 Nef domains required for disruption of major histocompatibility complex class I trafficking are also necessary for coprecipitation of Nef with HLA-A2. *J. Virol.* 79:632–636. http://dx.doi.org/10.1128/JVI.79.1.632-636.2005

Wonderlich, E.R., M. Williams, and K.L. Collins. 2008. The tyrosine binding pocket in the adaptor protein 1 (AP-1) mu1 subunit is necessary for Nef to recruit AP-1 to the major histocompatibility complex class I cytoplasmic tail. *J. Biol. Chem.* 283:3011–3022. http://dx.doi.org/10.1074/jbc.M707760200

Wonderlich, E.R., J.A. Leonard, D.A. Kulpa, K.E. Leopold, J.M. Norman, and K.L. Collins. 2011. ADP ribosylation factor 1 activity is required to recruit AP-1 to the major histocompatibility complex class I (MHC-I) cytoplasmic tail and disrupt MHC-I trafficking in HIV-1-infected primary T cells. *J. Virol.* 85:12216–12226. http://dx.doi.org/10.1128/JVI.00056-11